

Bootstrapped Control Limits for Score-Based Concept Drift Control Charts

Jiezhong Wu

Department of Industrial Engineering and Management Sciences,
Northwestern University

and

Daniel W. Apley

Department of Industrial Engineering and Management Sciences,
Northwestern University

January 13, 2026

Abstract

Monitoring for changes in a predictive relationship represented by a fitted supervised learning model (i.e., concept drift detection) is a widespread problem in modern data-driven applications. A general and powerful Fisher score-based concept drift approach was recently proposed by [Zhang et al. \(2023\)](#), in which detecting concept drift reduces to detecting changes in the mean of the model's score vector using a multivariate exponentially weighted moving average (MEWMA). To implement the approach, the initial data must be split into two subsets. The first subset serves as the training sample to which the model is fit, and the second subset serves as an out-of-sample test set from which the MEWMA control limit (CL) is determined. In this paper, we retain the same score-based MEWMA monitoring statistic as [Zhang et al. \(2023\)](#) and focus instead on improving the computation of the control limit. We develop a novel nested bootstrap procedure for calibrating the CL that allows the entire initial sample to be used for model fitting, thereby yielding a more accurate baseline model while eliminating the need for a large holdout set. We show that a standard nested bootstrap substantially underestimates the variability of the monitoring statistic and develop a 0.632-like correction that appropriately accounts for this. We demonstrate the advantages with numerical examples.

Keywords: Control charts, Concept drift, Bootstrap, Predictive modeling, Machine learning

1 Introduction

The increasing reliance on data-driven decision making has led to the widespread adoption of supervised learning models across various domains. These models aim to capture the predictive relationship $\mathbb{P}(Y|\mathbf{X})$ between a response variable Y and covariates \mathbf{X} . However, a fundamental challenge arises when the predictive relationship in new data deviates from that used to train the model, potentially rendering the model’s predictions unreliable or obsolete (Webb et al. 2016, Zhang et al. 2023, Malinovskaya et al. 2024), and/or reflecting a change in process behavior that should be detected. This challenge is particularly acute in domains like finance (Sun et al. 2017) and healthcare analytics (Razak et al. 2023), as most AI systems and algorithms require training data that may contain inherent biases or may not remain representative of the broader population over time (Barocas et al. 2023).

Statistical process monitoring (SPM) and control charts have long served as foundational tools for detecting changes in process characteristics over time (Montgomery 2020). The field has evolved considerably, with recent advances incorporating machine learning methods like kernel methods (Apsemidis et al. 2020) and neural networks (Psarakis 2011) to enhance monitoring capabilities. As datasets have grown larger and organizations increasingly rely on predictive models, the predictive relationship between variables has emerged as a critical characteristic that requires monitoring for quality control purposes, alongside traditional process variables monitoring.

This evolution in the goals of monitoring reflects a fundamental shift in how data are used in practice and/or represents a change in process behavior that should be detected. While traditional SPM methods are designed to detect shifts in the distribution of process variables, modern applications often require understanding changes in the predictive relationships themselves. This phenomenon, known as concept drift in the machine learning literature, occurs when the relationship between input features \mathbf{X} and the target variable Y evolves

over time (Webb et al. 2016), potentially degrading model performance (Moreno-Torres et al. 2012, Webb et al. 2016, Žliobaitė et al. 2016) and/or representing a change in process behavior that should be detected. These changes can manifest gradually or abruptly, and may not affect predictive accuracy immediately (Gama et al. 2014), making them difficult to detect using conventional methods.

Most existing concept drift detection methods fall into two categories, with each having significant limitations. The first category consists of error-based approaches that rely primarily on monitoring classification error rates or prediction accuracy metrics (Baena-García et al. 2006, Ross et al. 2012). While straightforward to implement, these methods often fail to detect concept drift when changes in $\mathbb{P}(Y|\mathbf{X})$ do not manifest as increased error rates, such as when decision boundaries shift in ways that maintain similar overall accuracy despite fundamental changes in the underlying relationship. The second category comprises adaptive learning algorithms, which continually retrain or update models to adapt to incoming data streams (Wang et al. 2003, Gama et al. 2014, Krawczyk et al. 2017). While these approaches can improve responsiveness, the adaptive model retraining also requires significant computation and may overfit transient changes.

Related to, but distinctly different from, concept drift detection, profile monitoring methods in statistical process control have been extensively developed to monitor functional relationships between response and predictor variables (Woodall et al. 2004). These methods typically involve monitoring regression parameters or fitted curves over time to detect changes in the relationship between a response variable and one or more explanatory variables (Chang & Yadama 2010, Abbasi et al. 2022). A profile in this context refers to the fitted functional relationship (e.g., a regression curve or model) that characterizes how Y depends on \mathbf{X} within a given batch of data. While this may appear similar to concept drift detection, profile monitoring fundamentally differs in its objectives, its approaches, and

the structure of the data to which it applies. In profile monitoring, data are grouped into batches of (\mathbf{X}, Y) observations, where some feature of $\mathbb{P}(Y|\mathbf{X})$ (typically $\mathbb{E}[Y|\mathbf{X}]$) for each batch represents a profile associated with the batch, and the objective is to monitor for changes in the nature of the profiles from batch to batch. This requires fitting predictive models separately to each batch of data. In contrast, in concept drift detection, data consist of individual, sequentially arriving (\mathbf{X}, Y) observations, and the objective is to detect whether the predictive relationship for new observations changes relative to what it was when a baseline model was fit to prior training data. Changes in the predictive relationship are detected by comparing a new stream of individual (\mathbf{X}, Y) observations to the baseline model, which does not involve fitting separate models to the new data.

Recently, [Zhang et al. \(2023\)](#) introduced a new Fisher score based concept drift detection that uses well-established statistical theory to show that detecting changes in $\mathbb{P}(Y|\mathbf{X})$ is equivalent to detecting changes in the mean of the score vector (the gradient of the log-likelihood) of the supervised learning model, a more familiar problem in SPM for which a conventional multivariate exponentially weighted moving average (MEWMA) control charts can be used. Their approach demonstrates superior detection power compared to traditional error-based concept drift methods, while also providing valuable diagnostic information to help understand the nature of detected changes. It also avoids having to continuously retrain the model, as in adaptive learning algorithms. Computing the MEWMA control limit (CL) in [Zhang et al. \(2023\)](#) requires that a second large sample of (\mathbf{X}, Y) observations be collected, in addition to the training sample to which the baseline model is fit. This can be achieved by splitting the training sample into two sets (with the baseline model fit to the first set, and the second set used to compute the CL), but this reduces the size of the data to which the baseline model is fit and generally requires very large sample sizes to accurately control false-alarm rate. This approach also shares conceptual similarities with

risk-adjusted monitoring in healthcare (Steiner et al. 2000), which monitors residuals from a risk model (typically a GLM). However, by using Fisher score vectors, the framework generalizes to any differentiable supervised learning model (including deep neural networks) without requiring the specific parametric forms used in risk-adjusted charts.

Our main contribution is that we present a more data-efficient and reliable approach that uses bootstrapping to compute the CL from the same training sample to which the baseline model is fit, thereby allowing the entire sample to be used to train a more accurate baseline model, as well as providing much more accurate control of false-alarm rate. For this we develop a nested bootstrap procedure with the inner loop accounting for future data variability and outer loop accounting for training sample variability. This is challenging because a naïve nested bootstrap procedure substantially underestimates variability of the MEWMA monitoring statistic for reasons that we discuss later. To account for this, we develop a 0.632-like (analogous to, but different from the original 0.632 correction of Efron (1983)) that controls false-alarm rate much more accurately than the two-sample CL calculation of Zhang et al. (2023), especially when the training sample size and/or the desired false-alarm rate is small. Our implementation takes advantage of the inherent parallelism in the nested bootstrap structure, making the method computationally efficient and practical for modern applications involving complex models like deep neural networks.

We note that the detection statistic utilized in our approach is identical to the score-based MEWMA statistic proposed by Zhang et al. (2023). Extensive empirical comparisons in Zhang et al. (2023) have already demonstrated that this statistic yields superior detection power compared to error-based methods (e.g., DDM (Gama et al. 2004), EDDM (Baena-García et al. 2006)) and adaptive windowing, particularly for drifts that do not immediately degrade prediction accuracy. Therefore, our numerical analysis focuses specifically on the accuracy of the proposed bootstrap Control Limits (Type I error control) and data efficiency,

rather than repeating the detection power comparisons established in prior literature.

The remainder of the paper is organized as follows. Section 2 reviews the score-based concept drift detection approach that is the basis of our approach. Section 3 develops a nested bootstrap approach and derives the associated variance-inflation correction that leads to appropriate CL. Section 4 demonstrates our method’s effectiveness through a variety of examples ranging from linear mixture models to complex nonlinear dynamical systems. Section 5 concludes with a summary of the main findings in this paper.

2 Background on Score-Based Concept Drift Detection

This work assumes a parametric supervised learning $g(\theta; \mathbf{X})$ is used to represent the conditional distribution $\mathbb{P}(Y|\mathbf{X};\theta)$ of the target variable Y given the input features $\mathbf{X} \in \mathbb{R}^p$, where θ denotes the parameters of the supervised learning, and p is the input dimension. For example, for classification problems, $g(\theta; \mathbf{X})$ directly outputs the response class probabilities; and for regression with Gaussian errors and squared-error loss, $g(\theta; \mathbf{X})$ represents the conditional mean $\mathbb{E}[Y|\mathbf{X};\theta]$ of a Gaussian $\mathbb{P}(Y|\mathbf{X};\theta)$. As in [Zhang et al. \(2023\)](#), we assume $g(\theta; \mathbf{X})$ is fit to the training data via maximum likelihood estimation (MLE), perhaps with regularization. This parametric assumption implies that the method is applicable to models such as generalized linear models (GLMs) and neural networks (where gradients with respect to weights are well-defined). It is not directly applicable to non-parametric or tree-based methods like Random Forests or XGBoost, which do not admit a differentiable likelihood function with respect to fixed parameters.

Denote the training data to which $g(\theta; \mathbf{X})$ is fit by $\{(\mathbf{x}_i, y_i) : i = 1, 2, \dots, n\}$, assumed to be an i.i.d. sample drawn from the joint distribution $\mathbb{P}(Y, \mathbf{X})$. For each observation

(\mathbf{x}_i, y_i) , the (Fisher) score vector is defined as $\mathbf{s}(\theta; \mathbf{x}_i, y_i) = \nabla_{\theta} \log \mathbb{P}(y_i | \mathbf{x}_i; \theta)$. Under certain regularity conditions, if the assumed parametric model is indeed the true data-generating mechanism with true parameters denoted by θ^0 , a fundamental result in statistical theory (Bickel & Doksum 2015)[Proposition 3.4.4] states that the expected value of the score vector, when evaluated at θ^0 , is equal to zero

$$\mathbb{E}_{\theta^0} [\mathbf{s}(\theta^0; \mathbf{X}, Y) | \mathbf{X}] = \int \mathbf{s}(\theta^0; \mathbf{X}, Y = y) \mathbb{P}(Y = y | \mathbf{X}; \theta^0) dy = \mathbf{0}. \quad (2.1)$$

In the context of machine learning, the notion of concept drift refers to the phenomenon where the underlying relationship between \mathbf{X} and Y evolves over time, which can be characterized as a shift in $\mathbb{P}(Y | \mathbf{X}; \theta)$. In the parametric setting of Zhang et al. (2023), concept drift translates to a change in θ . Under certain identifiability conditions, when the parameters change (to some $\theta \neq \theta^0$), the score vector mean $\mathbb{E}_{\theta}[\mathbf{s}(\theta^0; \mathbf{X}, Y) | \mathbf{X}] = \int \mathbf{s}(\theta^0; \mathbf{X}, Y = y) \mathbb{P}(Y = y | \mathbf{X}; \theta) dy$ will differ from zero. In light of this, the approach of Zhang et al. (2023) converts concept drift monitoring to the equivalent problem of monitoring for a change in the mean of the score vector $\mathbf{s}(\hat{\theta}; \mathbf{X}, Y)$, where $\hat{\theta}$ denotes the MLE of θ^0 obtained by fitting the model $g(\theta; \mathbf{X})$ to the training data. The MLE is given by

$$\hat{\theta} := \operatorname{argmax}_{\theta} \frac{1}{n} \sum_{i=1}^n \log \mathbb{P}(y_i | \mathbf{x}_i; \theta), \quad (2.2)$$

in which case

$$\nabla_{\theta} \frac{1}{n} \sum_{i=1}^n \log \mathbb{P}(y_i | \mathbf{x}_i; \theta) |_{\theta=\hat{\theta}} = \frac{1}{n} \sum_{i=1}^n \mathbf{s}(\hat{\theta}; \mathbf{x}_i, y_i) = \mathbf{0}, \quad (2.3)$$

which is the empirical counterpart of (2.1), since it represents the average score vector over the training data.

The empirical counterpart (2.3) also provides some intuition for why the score-based

concept drift monitoring approach can remain effective even when the parametric supervised learning model $g(\theta; \mathbf{X})$ is only an approximation to the true predictive relationship $\mathbb{P}(Y | \mathbf{X})$. Suppose the predictive relationship between Y and \mathbf{X} for a new set of data $\{(\mathbf{x}_{n+i}, y_{n+i}) : i = 1, 2, \dots, m\}$ differs substantially from what it was over the training data. The value of θ that minimizes the log-likelihood over the new data will generally differ from the MLE $\hat{\theta}$ over the training data, in which case

$$\nabla_{\theta} \frac{1}{m} \sum_{i=1}^m \log \mathbb{P}(y_{n+i} | \mathbf{x}_{n+i}; \theta) |_{\theta=\hat{\theta}} = \frac{1}{m} \sum_{i=1}^m \mathbf{s}(\hat{\theta}; \mathbf{x}_{n+i}, y_{n+i}), \quad (2.4)$$

will differ from zero. This argument does not require the supervised learning model to be correctly specified. Even under model misspecification, the maximum likelihood estimator converges to a pseudo-true parameter minimizing the Kullback–Leibler divergence. When the underlying predictive relationship changes, this pseudo-true parameter typically shifts, implying that the expected score vector evaluated at the original training fit is no longer zero. The same arguments hold if one uses a regularized version of MLE with the score vectors replaced by the derivative of the regularized log-likelihood, which is common in practice. This robustness property is supported by the empirical results in [Zhang et al. \(2023\)](#) and subsequent follow-ups, including applications to microstructure image data in [Zhang et al. \(2021\)](#) (for which the supervised learning model is always only an approximate representation of the true relationship). It is also demonstrated in our nonlinear oscillator example (Section 4.2), where a simplified neural network only approximates the complex physical dynamics but still allows changes in the physical parameters to be successfully detected. Theorem 3.4 formalizes this detectability argument under model misspecification. This was the basis for the concept drift monitoring approach of [Zhang et al. \(2023\)](#), who used a standard multivariate EWMA (MEWMA) to monitor for changes in the mean of the score vector as the new data are collected. To determine the CL for the MEWMA,

they divide the training data $\mathcal{D} = \{(\mathbf{x}_i, y_i) : i = 1, 2, \dots, n\}$ into two subsets: $\mathcal{D}_1 := \{(\mathbf{x}_i, y_i) : i = 1, 2, \dots, n_1\}$ and $\mathcal{D}_2 := \{(\mathbf{x}_i, y_i) : i = n_1 + 1, n_1 + 2, \dots, n\}$. The first subset, \mathcal{D}_1 , is used to fit the supervised learning model $g(\hat{\theta}; \mathbf{x})$, producing the MLE $\hat{\theta}$. They then compute the score vectors $\mathbf{s}(\hat{\theta}; \mathbf{x}_i, y_i)$ over the second subset, \mathcal{D}_2 , and apply an MEWMA to these score vectors to empirically compute the CL. Specifically, the CL is taken to be the $1 - \alpha$ (α is the desired false-alarm rate) sample quantile of the Hotelling T^2 statistics, $\{(\mathbf{z}_i - \bar{\mathbf{s}})^\top \widehat{\Sigma}^{-1} (\mathbf{z}_i - \bar{\mathbf{s}}) : i = n_1 + 1, n_1 + 2, \dots, n\}$, where $\bar{\mathbf{s}} = \sum_{i=n_1+1}^n \mathbf{s}(\hat{\theta}; \mathbf{x}_i, y_i) / (n - n_1)$ and $\widehat{\Sigma} = \sum_{i=1}^{n_1} (\mathbf{s}(\hat{\theta}; \mathbf{x}_i, y_i) - \bar{\mathbf{s}})(\mathbf{s}(\hat{\theta}; \mathbf{x}_i, y_i) - \bar{\mathbf{s}})^\top / n_1$ are the mean vector and covariance matrix of the score vectors for the second subset, and the MEWMA \mathbf{z}_i is defined recursively for $i = n_1 + 1, n_1 + 2, \dots$ via $\mathbf{z}_i = \lambda \mathbf{s}_i + (1 - \lambda) \mathbf{z}_{i-1}$, where λ is the MEWMA smoothing parameter.

The method of [Zhang et al. \(2023\)](#) was primarily intended for situations in which n is very large, since the size of \mathcal{D}_2 must be quite large to accurately determine the T^2 CL using the above procedure. Our nested bootstrap procedure (described in [Section 3](#)) to compute the T^2 CL results in much more accurate false-alarm rate control. This is especially true when n is not sufficiently large and/or the desired false-alarm rate is small, because the method of [Zhang et al. \(2023\)](#) requires a very large \mathcal{D}_2 for small false-alarm rates (FAR) (e.g., for a desired false-alarm rate of 0.001, the size of \mathcal{D}_2 must be much larger than 1,000). Moreover, our procedure allows the CL to be computed from the same data to which the supervised learning model is fit. This removes the need to divide the training sample into two subsets and allows the entire sample \mathcal{D} to be used for model fitting, which results in a more accurate model.

Practitioners often encounter scenarios where concept drift affects the relationship between Y and only a subset of the feature vector \mathbf{X} (e.g., the example in [Section 4.2](#), later). In such cases, the true parameters associated with the unaffected features may remain constant,

while those associated with the drifting features change. Because the score vector $\mathbf{s}(\hat{\theta}; \mathbf{x}, y)$ contains components for all model parameters, and the MEWMA statistic T^2 aggregates deviations across the entire parameter vector space, the method can detect these partial shifts. The detection power will of course depend on how strongly the drifting subset influences the overall likelihood.

3 Nested Bootstrap Procedure for Computing the CL

Suppose the training sample $\mathcal{D} = \{(\mathbf{x}_i, y_i)\}_{i=1}^n$ is drawn i.i.d. from some joint distribution $\mathbb{P}_0(Y, \mathbf{X})$ for which the conditional distribution $\mathbb{P}(Y|\mathbf{X}; \theta^0)$ can be implicitly represented by the parametric family $g_\gamma(\theta; \mathbf{x})$ of supervised learning models, where γ denotes fixed hyperparameters or regularization constants. Let $\mathbb{E}_0[\cdot]$ denote the expectation operator with respect to $\mathbb{P}_0(Y, \mathbf{X})$.

We apply the supervised learning model to the training dataset \mathcal{D} and compute the score vectors. For notational simplicity, we denote these score vectors as $\mathcal{S} = \{\mathbf{s}_i : i = 1, 2, \dots, n\}$ instead of using the functional notation $\mathbf{s}(\hat{\theta}; \mathbf{x}_i, y_i)$ from previous sections. Recall, each \mathbf{s}_i is the derivative of the component of the model fitting objective function (the negative log-likelihood or a regularized version, with no optimization constraints) associated with observation (\mathbf{x}_i, y_i) . Let $\bar{\mathbf{s}} = 1/n \sum_{i=1}^n \mathbf{s}_i$ and $\widehat{\Sigma} = 1/n \sum_{i=1}^n (\mathbf{s}_i - \bar{\mathbf{s}})(\mathbf{s}_i - \bar{\mathbf{s}})^\top$ denote the sample mean vector and covariance matrix of \mathcal{S} , respectively. By construction, $\bar{\mathbf{s}} = \mathbf{0}$.

Now we consider a set of new observations $\mathcal{D}^{\text{new}} = \{(\mathbf{x}_{n+i}, y_{n+i}) : i = 1, 2, \dots\}$ drawn i.i.d. from the same distribution as \mathcal{D} , to represent the situation that there is no shift in the predictive distribution. The score vector $\mathbf{s}_{n+i} = \mathbf{s}(\hat{\theta}; \mathbf{x}_{n+i}, y_{n+i})$ for each new observation depends on $(\mathbf{x}_{n+i}, y_{n+i}, \hat{\theta})$. Let $\mathcal{S}^{\text{new}} = \{\mathbf{s}_{n+i} : i = 1, 2, \dots\}$ denote the new score vectors, and note that \mathcal{S}^{new} depends on \mathcal{D} only via the fitted model parameters $\hat{\theta}$. Although the regularization parameters are also estimated from \mathcal{D} , we treat them as fixed for tractabil-

ity and use the same values when fitting all models within the bootstrapping procedure described below. Consequently, conditioned on $\hat{\theta}$, \mathcal{S}^{new} constitutes an i.i.d. sample with each \mathbf{s}_{n+i} , $i = 1, 2, \dots$, having some common mean $(\hat{\theta})$ and covariance matrix $\mathbf{V}(\hat{\theta})$ that are deterministic functions of $\hat{\theta}$, which we denote by

$$\mathbf{s}_{n+i} | \hat{\theta} \sim \text{i. i. d.}((\hat{\theta}), \mathbf{V}(\hat{\theta})), \quad i = 1, 2, \dots. \quad (3.1)$$

Although $\bar{\mathbf{s}} = \mathbf{0}$, it is not the case that $(\hat{\theta}) = \mathbf{0}$, because of estimation error in $\hat{\theta}$ and because \mathbf{s}_{n+i} are computed for new observations independent of the training data \mathcal{D} to which $g_\gamma(\hat{\theta}; \mathbf{x})$ is fit. For similar reasons, $\hat{\Sigma}$ should not be viewed as an estimator of $\mathbf{V}(\hat{\theta})$.

Let $\{\mathbf{z}_{n+i} : i = 1, 2, \dots\}$ denote the MEWMAs of the score vectors in \mathcal{S}^{new} , defined recursively as $\mathbf{z}_{n+i} = \lambda \mathbf{s}_{n+i} + (1 - \lambda) \mathbf{z}_{n+i-1}$, where $\lambda \in (0, 1)$ is the smoothing parameter and $\mathbf{z}_n = \mathbf{0}$. Write $\mathbf{z}_{n+i} = \lambda[\mathbf{s}_{n+i} + (1 - \lambda)\mathbf{s}_{n+i-1} + (1 - \lambda)^2\mathbf{s}_{n+i-2} + \dots + (1 - \lambda)^{i-1}\mathbf{s}_{n+1}]$ for $i = 1, 2, \dots$. From (3.1), conditioned on $\hat{\theta}$, the conditional mean and covariance of \mathbf{z}_{n+i} are

$$\mathbb{E}_0[\mathbf{z}_{n+i} | \hat{\theta}] = [1 - (1 - \lambda)^i] \mu(\hat{\theta}), \quad \text{Cov}_0[\mathbf{z}_{n+i} | \hat{\theta}] = \frac{\lambda}{2 - \lambda} [1 - (1 - \lambda)^{2i}] \mathbf{V}(\hat{\theta}). \quad (3.2)$$

The derivations in the remainder of this section relate the distribution of \mathbf{z}_{n+i} (for each $i = 1, 2, \dots$) to the distribution of analogous MEWMA ($\mathbf{z}_i^{b,j}$ from Step IV (b) of Algorithm 1) on the bootstrapped score vectors, in order to determine the CL for the T^2 chart on $\{\mathbf{z}_{n+i} : i = 1, 2, \dots\}$ as a function of i . Algorithm 1 provides an overview of our nested bootstrapping procedure to compute the CL. For each outer bootstrap replicate b ($= 1, 2, \dots, B_O$), let $\mathcal{D}^b = \{(\mathbf{x}_i^b, y_i^b) : i = 1, 2, \dots, n\}$ denote the bootstrap sample of size n from \mathcal{D} , and let $\mathcal{D}_{OOB}^b = \{(\mathbf{x}_{\text{OOB},i}^b, y_{\text{OOB},i}^b) : i \in \text{OOB}^b\}$ denote the corresponding out-of-bag (OOB) observations, where OOB^b represents the indices of observations in \mathcal{D} that are not selected in bootstrap sample b . The score vectors computed from these samples are denoted as

$\mathcal{S}^b = \{\mathbf{s}_i^b : i = 1, 2, \dots, n\}$ and $\mathcal{S}_{OOB}^b = \{\mathbf{s}_{OOB,i}^b : i \in OOB^b\}$ respectively, where $\mathbf{s}_i^b = \mathbf{s}(\hat{\theta}^b; \mathbf{x}_i^b, y_i^b)$, $\mathbf{s}_{OOB,i}^b = \mathbf{s}(\hat{\theta}^b; \mathbf{x}_{OOB,i}^b, y_{OOB,i}^b)$, and $\hat{\theta}^b$ are the parameters of the model fit to \mathcal{D}^b in Step 3-II of Algorithm 1. Let $\bar{\mathbf{s}}^b = 1/n \sum_{i=1}^n \mathbf{s}_i^b$ and $\hat{\Sigma}^b = 1/n \sum_{i=1}^n (\mathbf{s}_i^b - \bar{\mathbf{s}}^b)(\mathbf{s}_i^b - \bar{\mathbf{s}}^b)^\top$ denote the sample mean vector and covariance matrix of \mathcal{S}^b . For each inner bootstrap replicate j ($= 1, 2, \dots, B_I$) within outer replicate b , we denote the bootstrap sample of score vectors drawn (with replacement) from \mathcal{S}_{OOB}^b as $\{\mathbf{s}_i^{b,j} : i = 1, 2, \dots\}$ and their corresponding MEWMA as $\mathbf{z}_i^{b,j}$ from Step IV(b) of Algorithm 1.

It is worth noting that standard control charting often targets a specific in-control Average Run Length (ARL). However, in the context of score-based monitoring with complex models, the monitoring statistic is not generated from a stationary process with known parameters, but depends on the finite-sample variability of the fitted model. Furthermore, calculating ARLs via Monte Carlo simulation for our approach is computationally prohibitive due to the nested bootstrap required at each time step. Therefore, Algorithm 1 is designed to control the pointwise false-alarm rate α at each monitoring instance i . This ensures that the probability of a false alarm at any specific time t is effectively bounded by α , a property validated empirically in Section 4.

Algorithm 1: Nested Bootstrap Algorithm for Control Chart Setup

Input: the full training sample \mathcal{D} ; user's desired false-alarm rate α ; and the

MEWMA parameter λ .

Result: the upper CL CL_i for $i = 1, 2, 3, \dots$.

- 1) Fit and tune a supervised learning model $g_\gamma(\hat{\theta}; \mathbf{x})$ to \mathcal{D} using cross validation (CV) to select hyperparameters γ .
- 2) Apply the model to compute the score vectors \mathcal{S} , and their sample mean $\bar{\mathbf{s}}$ and covariance matrix $\widehat{\Sigma}$.
- 3) Using the following nested bootstrapping procedure, determine CL $\{CL_i : i = 1, 2, 3, \dots\}$ for the T^2 statistic.

For $b = 1, 2, \dots, B_O$ (outer bootstrap loop):

- I. Draw a bootstrap sample \mathcal{D}^b of size n from \mathcal{D} , and identify the OOB observations \mathcal{D}_{OOB}^b .
- II. Using the same tuning parameters γ from Step 1, fit a new model $g_\gamma(\hat{\theta}^b; \mathbf{x})$ to \mathcal{D}^b .
- III. Compute the score vectors \mathcal{S}^b and \mathcal{S}_{OOB}^b , and the sample mean $\bar{\mathbf{s}}^b$ and covariance matrix $\widehat{\Sigma}^b$ of \mathcal{S}^b .
- IV. For $j = 1, 2, \dots, B_I$ (inner bootstrap loop):
 - (a) Draw a bootstrap sample of score vectors $\{\mathbf{s}_i^{b,j} : i = 1, 2, 3, \dots\}$ from \mathcal{S}_{OOB}^b .
Initialize $\mathbf{z}_0^{b,j} = \mathbf{0}$.
 - (b) For $i = 1, 2, 3, \dots$, compute the MEWMA $\mathbf{z}_i^{b,j} = \lambda \mathbf{s}_i^{b,j} + (1 - \lambda) \mathbf{z}_{i-1}^{b,j}$ and the T^2 statistic in (3.5).

For each $i = 1, 2, 3, \dots$, set CL_i to be the upper α quantile of

$$\{T_i^{b,j} : b = 1, 2, \dots, B_O; j = 1, 2, \dots, B_I\}.$$

Within the nested bootstrap procedure, each outer bootstrap sample \mathcal{D}^b in Step 3-I assumes the role of the original training sample \mathcal{D} and accounts for Phase I (model-estimation) uncertainty arising from fitting the supervised learning model, i.e., variability in $\hat{\theta}$. The

corresponding out-of-bag (OOB) sample $\mathcal{D}_{\text{OOB}}^b$ plays the role of the future data stream \mathcal{D}^{new} and captures Phase II (prospective monitoring) variability in incoming observations. As a result, Algorithm 1 is designed to control the marginal pointwise false-alarm rate at each monitoring time, explicitly accounting for both Phase I uncertainty (via the outer bootstrap loop) and Phase II data variability (via the inner bootstrap loop). In contrast, a single (non-nested) bootstrap procedure would account only for Phase II variability and therefore substantially underestimate the control limit. Let n^b denote the number of unique observations in \mathcal{D} sampled in \mathcal{D}^b , in which case $|\mathcal{D}_{\text{OOB}}^b| = n - n^b$.

We employ standard bootstrap sampling with replacement. Consequently, each bootstrap sample \mathcal{D}^b contains approximately $1 - (1 - 1/n)^n \approx 0.632$ fraction of unique observations from \mathcal{D} (Efron 1983). The remaining $\approx 0.368n$ observations form the out-of-bag (OOB) sample $\mathcal{D}_{\text{OOB}}^b$, which serves as a proxy for independent future data. For notational simplicity, in the following derivations we assume each $n^b = 0.632n$.

Remark 3.1. *For each $i = 1, 2, \dots$, one might consider using the empirical distribution of a naïve version of the bootstrapped T^2 statistics $\{(\mathbf{z}_i^{b,j} - \bar{\mathbf{s}}^b)^\top (\widehat{\Sigma}^b)^{-1} (\mathbf{z}_i^{b,j} - \bar{\mathbf{s}}^b) : b = 1, 2, \dots, B_O; j = 1, 2, \dots, B_I\}$ to approximate the distribution of the T^2 statistic $T_{n+i} = (\mathbf{z}_{n+i} - \bar{\mathbf{s}})^\top \widehat{\Sigma}^{-1} (\mathbf{z}_{n+i} - \bar{\mathbf{s}})$ for \mathcal{S}^{new} and compute its CL. However, this naïve bootstrap distribution can be severely biased due to the finite sample size of $\mathcal{S}_{\text{OOB}}^b$, for reasons that become clear later (also see Remark 3.3 below). The following derivations account for this bias and result in CLs that accurately control false-alarm rate.*

3.1 Covariance Inflation and Control Limit Construction

To ensure the validity of the proposed control limits, we require specific regularity assumptions and intermediate results regarding the moments of the MEWMA statistics. The detailed theoretical framework, including formal assumptions, intermediate lemmas, and

their proofs, is provided in Appendix A.

The main result of these derivations is that the bootstrap MEWMA statistic is a stochastically inflated version of the true MEWMA statistic. This motivates the scaling factor $k(\lambda, i, n)$ presented below.

Theorem 3.1 (Covariance inflation factor). *Suppose Assumptions A.1 and A.2 (see Appendix A) hold, and the functions $\mu(\theta)$ and $\mathbf{V}(\theta)$ are differentiable in a neighborhood of θ_0 . Then, for each $i \geq 1$, the unconditional covariance of the bootstrap MEWMA statistic $\mathbf{z}_i^{b,j}$ is inflated relative to that of the true MEWMA statistic \mathbf{z}_i by the scalar factor*

$$k(\lambda, i, n) = \frac{\frac{\lambda}{2-\lambda}[1 - (1-\lambda)^{2i}] + \frac{3.72}{n}[1 - (1-\lambda)^i]^2}{\frac{\lambda}{2-\lambda}[1 - (1-\lambda)^{2i}] + \frac{1}{n}[1 - (1-\lambda)^i]^2}, \quad (3.3)$$

in the sense that

$$\text{Cov}_0[\mathbf{z}_i^{b,j}] \cong k(\lambda, i, n) \text{Cov}_0[\mathbf{z}_i]. \quad (3.4)$$

Theorem 3.1 implies that dividing the bootstrap MEWMA statistic by $\sqrt{k(\lambda, i, n)}$ produces a variance-corrected quantity whose covariance matches that of the true in-control MEWMA statistic. This leads to the following procedure for determining the Control Limits.

Corollary 3.2 (Variance-corrected bootstrap T^2 and control limits). *Let $k(\lambda, i, n)$ be as in (3.3) and define the variance-corrected bootstrap MEWMA statistic $\tilde{\mathbf{z}}_i^{b,j} = \mathbf{z}_i^{b,j} / \sqrt{k(\lambda, i, n)}$. For each monitoring time $i \geq 1$, define the bootstrap Hotelling T^2 statistics*

$$T_i^{b,j} = (\tilde{\mathbf{z}}_i^{b,j} - \bar{\mathbf{s}}^b)^\top (\hat{\Sigma}^b)^{-1} (\tilde{\mathbf{z}}_i^{b,j} - \bar{\mathbf{s}}^b), \quad (3.5)$$

and take the CL CL_i to be the empirical upper $(1-\alpha)$ quantile of $\{T_i^{b,j} : b = 1, \dots, B_O, j =$

$1, \dots, B_I\}$. Then the resulting MEWMA chart applied to

$$T_{n+i} = (\mathbf{z}_{n+i} - \bar{\mathbf{s}})^\top \hat{\Sigma}^{-1} (\mathbf{z}_{n+i} - \bar{\mathbf{s}}) \quad (3.6)$$

has point-wise false-alarm probability approximately α at each time i under \mathbb{P}_0 .

After the CLs are obtained, monitoring proceeds in the usual way. For each new incoming observation $(\mathbf{X}_{n+i}, Y_{n+i})$, compute its score vector, update the MEWMA statistic \mathbf{z}_{n+i} , and compare the corresponding T_{n+i} value to CL_i . A signal is issued at the first time i for which $T_{n+i} > \text{CL}_i$.

3.2 Stabilization and Detectability of the Control Limit

Throughout the remainder of this section, recall that \mathcal{D} denotes the fixed Phase I training sample. Let T_i^* denote a generic bootstrap replicate of the monitoring statistic at time i , constructed according to the resampling scheme in Algorithm 1 and Corollary 3.2. Conditional on \mathcal{D} , let $F_i(\cdot | \mathcal{D})$ denote the distribution function of T_i^* , which accounts for both Phase I estimation uncertainty and Phase II variability, and let $q_{i,\alpha}(\mathcal{D})$ be its $(1 - \alpha)$ quantile. To describe the steady-state behavior, define T_∞^* to be the stationary analogue of T_i^* obtained by applying the same recursion to a stationary (two-sided) bootstrap score sequence. Let $F_\infty(\cdot | \mathcal{D})$ denote the conditional distribution of T_∞^* given \mathcal{D} , and let $q_{\infty,\alpha}(\mathcal{D})$ denote its $(1 - \alpha)$ quantile.

Because the MEWMA statistic is initialized at zero, the bootstrap control limits CL_i defined in Corollary 3.2 are time-varying at early monitoring times. In long monitoring runs, however, recomputing the control limit indefinitely is computationally inefficient. The following result shows that the bootstrap control limit stabilizes geometrically fast as the monitoring time increases.

Theorem 3.3 (Stabilization of the bootstrap control limit). *Assume Assumptions A.1–A.4 hold and that there is no concept drift. In addition, assume that the limiting bootstrap distribution $F_\infty(\cdot | \mathcal{D})$ of T_∞^* admits a density $f_\infty(\cdot | \mathcal{D})$ such that: (i) $f_\infty(q_{\infty,\alpha}(\mathcal{D}) | \mathcal{D}) \geq c_0(\mathcal{D}) > 0$, for some constant $c_0(\mathcal{D})$, and (ii) $f_\infty(\cdot | \mathcal{D})$ is bounded in a neighborhood of $q_{\infty,\alpha}(\mathcal{D})$. Then $q_{\infty,\alpha}(\mathcal{D})$ is finite and*

$$|q_{i,\alpha}(\mathcal{D}) - q_{\infty,\alpha}(\mathcal{D})| \leq C(\mathcal{D})(1 - \lambda)^i \quad \text{for all } i \geq 1,$$

where $C(\mathcal{D}) < \infty$ depends only on the Phase I training sample \mathcal{D} .

Remark 3.2. *Theorem 3.3 establishes geometric stabilization for the population bootstrap quantile $q_{i,\alpha}(\mathcal{D})$. In practice, Algorithm 1 computes the control limit CL_i as an empirical $(1 - \alpha)$ quantile based on $B_O \times B_I$ bootstrap replicates, which introduces additional Monte Carlo variability. Because Phase I uncertainty is captured by the outer bootstrap loop, the effective number of independent outer draws is B_O , and the Monte Carlo error is therefore typically dominated by an $O_p(B_O^{-1/2})$ term. The numerical results in Section 4, obtained with $B_O = 100$ and $B_I = 200$, indicate that this Monte Carlo error is negligible for practical purposes.*

Remark 3.3. *Equation (3.4) implies that $\text{Cov}_0[\mathbf{z}_i^{b,j}] = \text{Cov}_0[\mathbf{z}_i] + [1 - (1 - \lambda)^i]^2 \mathbf{I}(\theta^0) / 0.368n$, where, from equation (A.8), the term $\mathbf{I}(\theta^0) / 0.368n$ ($\mathbf{I}(\theta^0)$ is the Fisher information matrix) in the difference is precisely $\mathbb{E}_0[\text{Cov}_0[\bar{\mathbf{S}}_{\text{OoB}}^b | \hat{\theta}^b]]$. Thus, this difference accounts for the variability in the mean $\bar{\mathbf{S}}_{\text{OoB}}^b$ of the “population” $\mathcal{S}_{\text{OoB}}^b$ (whose cardinality is $0.368n$) from which the inner bootstrap samples are drawn in Algorithm 1. This constitutes a nuanced instantiation of the 0.632 bootstrap rule that is crucial for obtaining a correct CL. When this correction is omitted (in which case the scaling factor $k(\lambda, i, n)$ in (3.5) is replaced by 1), we have observed empirically that the bootstrapped CL is typically far too large and the detection power is unnecessarily compromised.*

The preceding results establish accurate control limit calibration for the proposed score-based MEWMA chart under correct model specification. We now investigate whether the score-based monitoring mechanism continues to detect changes in the predictive relationship when the supervised learning model is misspecified. In particular, we focus on whether a distributional shift induces a nonzero mean in the monitored score vector, which is the fundamental signal driving detection. Let \mathbb{P}_0 denote the in-control joint distribution of (\mathbf{X}, Y) , and let $p_\theta(y | \mathbf{x})$ denote the working conditional density (possibly misspecified). Define the pseudo-true parameter $\theta^* := \arg \max_{\theta \in \Theta} \mathbb{E}_{\mathbb{P}_0}[\log p_\theta(Y | \mathbf{X})]$, and let $\mathbf{s}(\theta; \mathbf{x}, y) := \nabla_\theta \log p_\theta(y | \mathbf{x})$ denote the corresponding score vector. For a post-change distribution $\mathbb{P}_1 \neq \mathbb{P}_0$, define θ_1^* analogously.

Theorem 3.4 (Detectability under model misspecification). *Assume that the pseudo-true parameters θ^* and θ_1^* are uniquely defined and satisfy the regularity conditions of Assumption A.3. Then*

- (a) *In-control score mean $\mathbb{E}_{\mathbb{P}_0}[\mathbf{s}(\theta^*; \mathbf{X}, Y)] = \mathbf{0}$.*
- (b) *If $\theta_1^* \neq \theta^*$, then $\mathbb{E}_{\mathbb{P}_1}[\mathbf{s}(\theta^*; \mathbf{X}, Y)] \neq \mathbf{0}$.*
- (c) *Under \mathbb{P}_1 , the MEWMA statistic constructed from $\mathbf{s}(\theta^*; \mathbf{X}, Y)$ converges geometrically in mean to a nonzero vector.*

Theorem 3.4 shows that detectability of concept drift does not rely on correct model specification. That is, any shift that changes the pseudo-true parameter produces a nonzero mean in the monitored score vector, yielding a detectable signal in the MEWMA statistic.

3.3 Practical Considerations and Computational Aspects

Several implementation aspects of the algorithm warrant further discussion. When fitting models to bootstrap samples in Step 3-II, it is important to use the same tuning parameters

γ that were selected in Step 1 rather than performing new CV, as this maintains consistency in the model structure across replicates. If the covariance matrices $\widehat{\Sigma}$ in Step 2 and $\widehat{\Sigma}^b$ in Step 3-III are poorly conditioned (e.g., when $\widehat{\theta}^b$ is high-dimensional and/or has highly correlated components), then $\epsilon\mathbf{I}$ for some small scalar ϵ should be added to them before they are inverted in (3.5) and (3.6). If this is done, it should be done consistently in Steps 2 and 3-III using the same value of ϵ . Note that $\widehat{\Sigma}^b$ will typically be more poorly conditioned than $\widehat{\Sigma}$, since there are fewer distinct score vectors in $\mathbf{S}_{\mathcal{D}}^b$ than in $\mathbf{S}_{\mathcal{D}}$. Thus, whether $\widehat{\Sigma}$ is replaced by $\widehat{\Sigma} + \epsilon\mathbf{I}$ in Step 2 should depend on how poorly conditioned the $\widehat{\Sigma}^b$ are in step 3-III.

The choice of monitoring parameters α and λ follows standard MEWMA practice. α is determined by the acceptable false-alarm rate, and λ balances the trade-off between detecting small, gradual shifts versus large, abrupt shifts (Montgomery 2020). For the bootstrap parameters, B_O governs the accuracy of estimating the variability due to model fitting, while B_I captures the variability of future data. Since B_O determines the number of model refits, it represents the primary computational constraint. However, we note that the B_O replicates are independent and can be efficiently performed simultaneously across multiple cores or GPUs. For deep learning models (like the one in Section 4.2), the refitting process can leverage GPU acceleration to significantly reduce runtime. For B_I , the inner-loop computations are relatively inexpensive. Accordingly, we recommend that practitioners choose B_I to be conservatively large (e.g., $B_I \geq 200$) and focus computational resources on maximizing B_O , which governs the dominant cost of model refitting.

Remark 3.4. *In some practical applications, new data may arrive in batches rather than as single observations. In such cases, we recommend randomly ordering the observations within the batch and processing them sequentially through the MEWMA recursion. Because the control limit CL_i is a function of the time index i relative to the start of monitoring*

(and the training data) but does not depend on the specific values of the new observations, the random ordering of a batch does not alter the threshold sequence.

After using Algorithm 1 to establish the CL, monitoring for concept drift in new observations is straightforward. Given each new observation $(\mathbf{x}_{n+i}, y_{n+i})$, we compute its score vector \mathbf{s}_i using the model $g_\gamma(\hat{\theta}; \mathbf{x})$, update the MEWMA statistic via $\mathbf{z}_{n+i} = \lambda \mathbf{s}_{n+i} + (1 - \lambda) \mathbf{z}_{n+i-1}$, and compute the T^2 monitoring statistics (3.6).

Concept drift is detected when T_{n+i} exceeds its corresponding CL CL_i . The choice of the MEWMA smoothing parameter λ also affects the monitoring sensitivity, and the tradeoff is the same as in any MEWMA monitoring procedure: Smaller values of λ provide more powerful eventual detection of large shifts but can delay the detection of large shifts, whereas larger values provide quicker detection of large shifts but may fail to detect smaller shifts.

4 Numerical Examples

To illustrate our approach and demonstrate its effectiveness at controlling the false-alarm rate, we present two numerical examples. The first is a more transparent example in which the predictive relationship $\mathbb{P}(Y | \mathbf{X})$ is a mixture of two simple linear relationships, and the second involves a more complex nonlinear predictive relationship.

4.1 Mixed Linear Population

The data-generating process for this example involves the two linear models

$$y_i = 16x_i + 5 + \varepsilon_i, \quad \varepsilon_i \sim \mathcal{NID}(0, 16), \quad (4.1)$$

and

$$y_i = 12x_i + 3 + \varepsilon_i, \quad \varepsilon_i \sim \mathcal{NID}(0, 16), \quad (4.2)$$

where predictor values x_i are uniformly sampled from $[-\sqrt{3}, \sqrt{3}]$. The training data of size $n = 2,000$ are generated exclusively from model (4.1), yielding an pre-shift sample governed by a single linear relationship. The future data to be monitored comprise 1,000 observations: the first 200 points (pre-shift) follow the same single linear model (4.1), while the remaining 800 points (post-shift) are generated from a mixture that draws y_i from either (4.1) or (4.2) with equal probability 0.5, representing a shift in $\mathbb{P}(Y|\mathbf{X})$.

We fit a linear predictive model $g_\gamma(\hat{\theta}; x) = \hat{\theta}_0 + \hat{\theta}_1 x$ via ridge regression with L_2 regularization parameter $\gamma = 0.1$ (i.e. with the loss function $\sum_{i=1}^n [(y_i - \mathbf{x}_i^\top \hat{\theta})^2 + \gamma \|\hat{\theta}\|^2 / n]$, for which the penalized log-likelihood for observation i is

$$\ell_{\text{pen}}(\hat{\theta}; \mathbf{x}_i, y_i) = \log \mathbb{P}(y_i | \mathbf{x}_i; \hat{\theta}) - \frac{\gamma}{2n} \|\hat{\theta}\|^2 = -\frac{1}{2} (y_i - \mathbf{x}_i^\top \hat{\theta})^2 - \frac{1}{2} \log(2\pi\sigma^2) - \frac{\gamma}{2n} \|\hat{\theta}\|^2.$$

The score vectors are therefore

$$\mathbf{s}(\hat{\theta}; \mathbf{x}_i, y_i) = (y_i - \mathbf{x}_i^\top \hat{\theta}) \mathbf{x}_i - \frac{\gamma}{n} \hat{\theta}. \quad (4.3)$$

We used MEWMA parameter $\lambda = 0.01$, which we chose via 5-fold CV, and desired pointwise false-alarm probability $\alpha = 0.001$. In Algorithm 1, we used $B_O = 100$ and $B_I = 200$.

In Figure 4.1, we visualize the transition from the pre-shift predictive relationship (4.1) to the post-shift relationship that is a mixture of (4.1) and (4.2). Although the shift appears quite small in Figure 4.1, Figure 4.2(a) demonstrates that it is still detectable. Figure 4.2(a) shows a typical evolution of our T^2 monitoring statistic over 1,000 observations, with the first 200 following the pre-shift distribution and the last 800 the post-shift distribution. The T^2 statistic remains below the CL prior to the shift and then begins to increase immediately following the shift at time 201 until it first exceeds the CL at time 258, demonstrating the method's ability to detect the shift. This behaviour aligns with our derivation in Section 3,

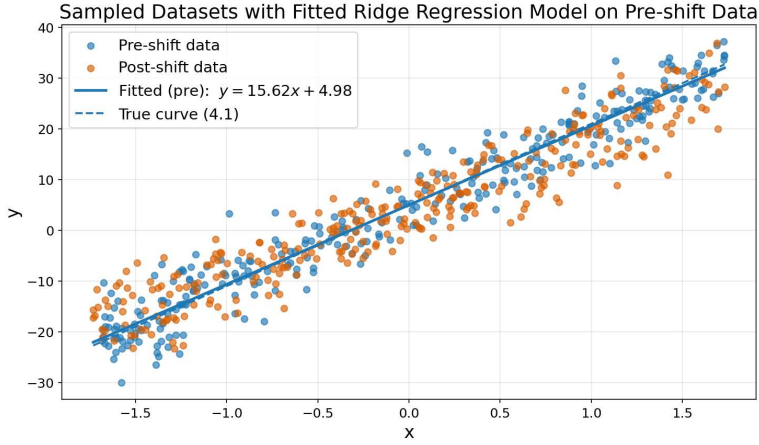


Figure 4.1: Visualization of predictive relationships for the linear example before and after the shift. The blue points are a scatter plot of y vs. x for the pre-shift single linear model (4.1), and the orange points correspond to the post-shift mixture model (4.1) and (4.2). The shift from a single component to a mixture alters $\mathbb{P}(Y|\mathbf{X})$, representing a structural shift in the predictive relationship that is relatively small but can still be detected by our approach.

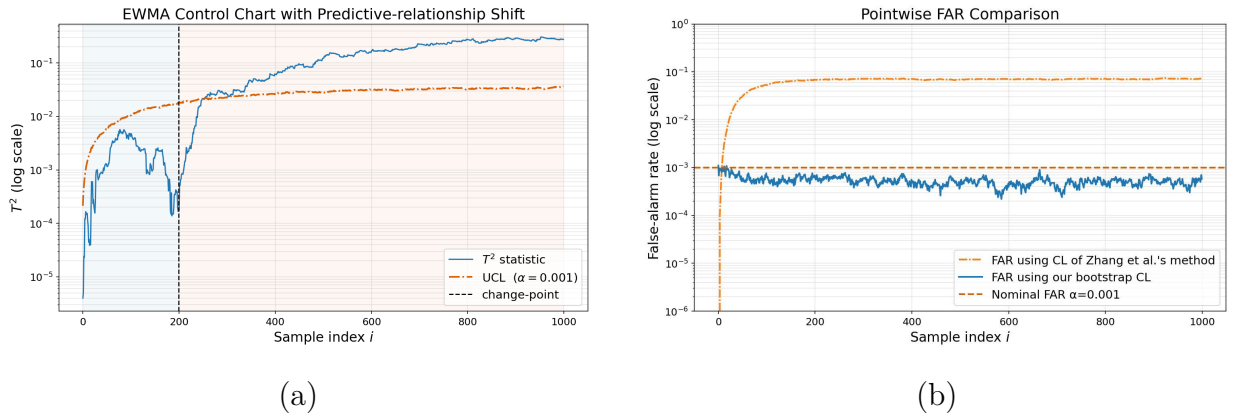


Figure 4.2: (a) Typical monitoring results using our bootstrap CL approach for the linear mixture example showing the detection of concept drift at new observation number 258 (the shift first occurred at observation number 201). The T^2 statistics (T_i from Eq. (3.6), represented by the blue line) remain below the control limit (dashed orange line) prior to the shift at observation 201, and sharply exceed it shortly after the shift. (b) Comparison of the pointwise false-alarm rate for our bootstrap CL (blue curve) versus the CL of Zhang et al. (2023) (orange curve) averaged over 50 database replicates under the pre-shift predictive relationship (4.1). Our bootstrap CL much more accurately maintains the empirical false-alarm rate close to the desired $\alpha = 0.001$.

where changes in $\mathbb{P}(Y|\mathbf{X})$ were shown to induce non-zero means in the score vectors.

To better assess the empirical false-alarm control, the blue curve in Figure 4.2(b) shows the pointwise false-alarm rate over the first 1,000 observations when no shift occurs, esti-

mated as the average pointwise false-alarm rate over 50 replicates. On each replicate, a different training data set was generated, the ridge regression model was fit to these data, Algorithm 1 was used to compute the CL as a function of time, a new set of 1,000 observations was generated from the same distribution (representing no shift), and then the T^2 statistic was computed for each new observation and compared to its CL to determine if there was a signal at that time. Our method consistently maintains the false-alarm rate at close to the desired value $\alpha = 0.001$. The orange curve shows the corresponding results from the baseline method of Zhang et al. (2023), which exhibits substantially inflated FAR exceeding 0.06, highlighting the more accurate false-alarm rate provided by bootstrap CL. The discrepancy arises for two reasons. First, Zhang et al. (2023) used a constant CL, because without bootstrapping there is no clear way to compute a time-varying CL. Second, Zhang et al. (2023) fit their model on only the first half of the training data and compute the constant CL from the second half. The resulting CL is based on a much smaller effective sample size than in our nested bootstrapping procedure and cannot reliably provide correct Type I error control unless the training sample size is quite large. In contrast, our approach provides accurate false-alarm rate control even with the relatively small training sample size of 2,000 in this example.

It should be noted that the intended application scenarios in Zhang et al. (2023) involved much larger training sample sizes and/or larger values for the desired α . For $\alpha = 0.01$ (for example), the method of Zhang et al. (2023) provides much more accurate false-alarm control than in this example with $\alpha = 0.001$. With $\alpha = 0.001$, the method of Zhang et al. (2023) generally requires that the size of the training subset used to compute the CL is at least 10,000 to accurately estimate the upper 0.001 quantile of the empirical distribution of the T^2 statistic. In this regard, our bootstrap CL approach can be viewed as an extension of Zhang et al. (2023) to smaller training sample sizes and/or larger desired α values.

4.2 Nonlinear Oscillator System

To demonstrate our method’s effectiveness in detecting changes in complex nonlinear predictive relationships, we consider a physics-based system that represents a variant of the two-degree-of-freedom nonlinear oscillator with a finite-extensibility coupling spring proposed by [Febbo & Machado \(2013\)](#). The system consists of two masses moving in one dimension, connected by nonlinear springs. Let $p_1(t)$ and $p_2(t)$ denote the positions at (continuous) time t of the two masses having masses m_1 and m_2 , respectively, and let $v_1(t) = \dot{p}_1(t)$ and $v_2(t) = \dot{p}_2(t)$ denote their velocities. The system evolves according to the following differential equations:

$$\begin{aligned}\ddot{p}_1(t) &= \frac{1}{m_1}(-k_1 p_1(t) - c_1 \dot{p}_1(t) + k_3 \phi(p_1(t), p_2(t))), \\ \ddot{p}_2(t) &= \frac{1}{m_2}(-k_2 p_2(t) - c_2 \dot{p}_2(t) - k_3 \phi(p_1(t), p_2(t))),\end{aligned}\tag{4.4}$$

where $\phi(p_1, p_2) = (p_1 - p_2)/(1 + |p_1 - p_2|)$ represents the nonlinear coupling force.

To generate the training data, we adopt an ensemble-based sampling scheme. For each observation i , the oscillator system in (4.4) is independently initialized with initial conditions $(p_1(0), v_1(0), p_2(0), v_2(0))$ drawn i.i.d. from a fixed distribution. The system is then evolved according to (4.4), and the state is recorded at a time t_i drawn uniformly from $[0, 30]$. This yields an i.i.d. training sample $\{(\mathbf{X}_i, y_i)\}_{i=1}^n$ with $n = 3,000$ observations.

The feature vector $\mathbf{X}_i \in \mathbb{R}^4$ corresponds to the system state at time t_i and is given by $\mathbf{X}_i = [p_1(t_i), v_1(t_i), p_2(t_i), v_2(t_i)]^\top$. The response variable y_i represents the total mechanical energy (kinetic plus potential) of the system at time t_i , given by

$$y_i = \frac{1}{2}(m_1 v_1^2(t_i) + m_2 v_2^2(t_i)) + \frac{1}{2}(k_1 p_1^2(t_i) + k_2 p_2^2(t_i)) + k_3 \phi(p_1(t_i), p_2(t_i)) + \varepsilon_i,\tag{4.5}$$

where $\varepsilon_i \sim \mathcal{NID}(0, \sigma^2)$ represents measurement noise. For the training data, we used the system parameters $m_1 = 1.0$, $m_2 = 2.0$, $k_1 = 1.0$, $k_2 = 2.0$, $k_3 = 1.5$, $c_1 = 0.1$, and $c_2 = 0.2$.

To simulate concept drift, we generate new observations from the same oscillator system but with modified physical parameters $m'_1 = 1.1m_1$, $m'_2 = 1.2m_2$, $k'_1 = 1.3k_1$, while holding the remaining parameters fixed. These changes represent interpretable real-world perturbations, such as increased mass (e.g., due to material accumulation) or stiffened springs (e.g., due to thermal effects), and they alter both the system’s natural frequencies and its energy landscape. As a result, the conditional distribution $\mathbb{P}(Y | \mathbf{X})$ is systematically shifted, inducing concept drift that our monitoring framework aims to detect.

To model the nonlinear predictive relationship, we fit a feed-forward multilayer perceptron (MLP) with $L = 4$ hidden layers of width $H = 32$ and ReLU activations, followed by a linear output layer. That is, the network has the form

$$h_0(\mathbf{x}) = \mathbf{x}, \quad h_\ell(\mathbf{x}) = \text{ReLU}(W_\ell h_{\ell-1}(\mathbf{x}) + \mathbf{b}_\ell) \quad (\ell = 1, \dots, L), \quad g_\gamma(\Theta; \mathbf{x}) = \mathbf{w}^\top h_L(\mathbf{x}) + b.$$

Here $W_\ell \in \mathbb{R}^{H \times H}$ and $\mathbf{b}_\ell \in \mathbb{R}^H$ denote the weights and biases of the ℓ th hidden layer (with $W_1 \in \mathbb{R}^{H \times 4}$), and (\mathbf{w}, b) are the parameters of the final linear output layer. This architecture has 3,361 trainable parameters in total, of which $H + 1 = 33$ correspond to the final layer.

Following [Zhang et al. \(2023\)](#), we monitor only the parameters of the final linear output layer, denoted by $\theta = (\mathbf{w}, b)$, while treating the parameters of the hidden (feature-extraction) layers $\Theta_{\text{feat}} = \{(W_\ell, \mathbf{b}_\ell)\}_{\ell=1}^L$ as fixed during monitoring. This strategy keeps the dimension of the score vector tractable even for deep architectures, while still capturing changes in the predictive relationship $\mathbb{P}(Y | \mathbf{X})$ that propagate through the network (see

also [Yosinski et al. \(2014\)](#)). When fitting the model to the training data, all parameters in Θ are estimated; however, for monitoring, inference is conducted with respect to θ only, using the penalized Gaussian log-likelihood

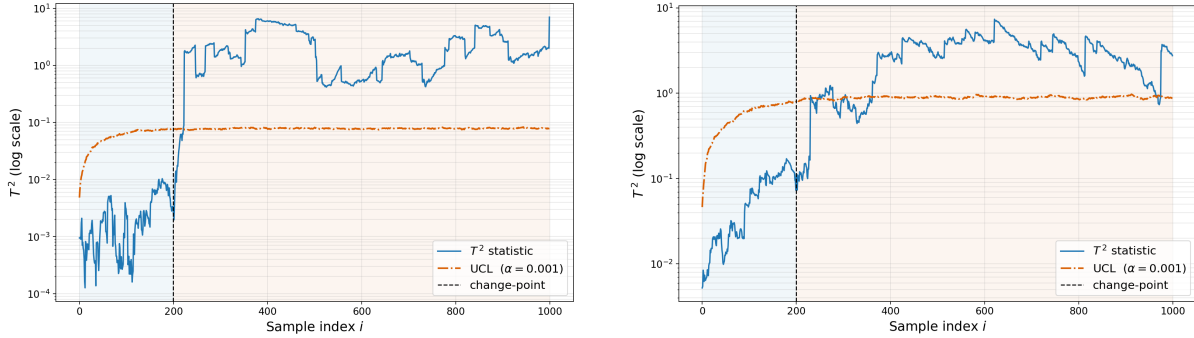
$$\ell_{\text{pen}}(\theta; \mathbf{x}_i, y_i) = -\frac{1}{2\sigma^2}(y_i - g_\gamma(\Theta; \mathbf{x}_i))^2 - \frac{1}{2}\log(2\pi\sigma^2) - \frac{\gamma}{2n}\|\theta\|^2,$$

with regularization parameter $\gamma = 10^{-1}$.

For each observation (\mathbf{x}_i, y_i) , the score vector is defined as the gradient of the penalized log-likelihood with respect to the monitored parameters θ , evaluated at the fitted values $\hat{\theta}$. Because the network architecture may be deep and highly nonlinear, we do not hand-code this gradient. Instead, the score vector is computed via automatic differentiation by calling `loss.backward()` in PyTorch. This implementation choice allows the proposed monitoring framework to scale seamlessly to modern deep neural networks without requiring analytic expressions for the score function.

After fitting the network on this baseline data, we run [Algorithm 1](#) with $B_O = 100$, $B_I = 200$, $\alpha = 0.001$, and $\lambda = 0.01$. The subsequent monitoring stream contains $M = 1,000$ observations, of which the final 800 incorporate the prescribed parameter shift. Additional implementation details, including our computational environment, are reported in [Appendix B](#).

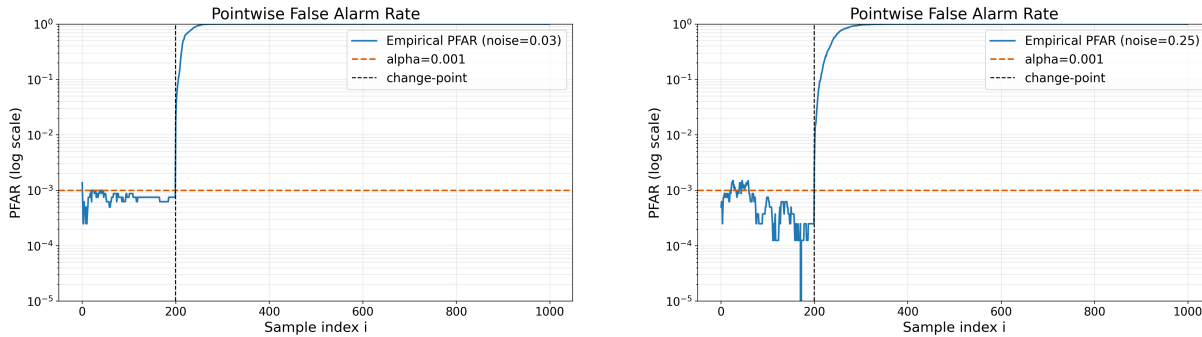
We consider two scenarios with different noise levels, the results for which are shown in [Figure 4.3](#) for a typical replicate. In the low-noise scenario ([Figure 4.3a](#); $\sigma = 0.03$), the fitted model has a CV R^2 of 0.975, and the T^2 statistic increases above the CL shortly after the distribution shifts at new observation 201. The T^2 statistic remains consistently above the CL after the shift, reflecting our method’s ability to reliably detect subtle changes in the system dynamics. The high-noise scenario ($\sigma = 0.25$) represents the situation that the



(a) Low noise ($\sigma = 0.03$, 5-fold CV $R^2 \approx 0.975$) (b) High noise ($\sigma = 0.25$, 5-fold CV $R^2 \approx 0.137$)

Figure 4.3: Typical monitoring results using our bootstrap CL approach for the coupled nonlinear oscillator system under (a) low-noise and (b) high-noise conditions. The shifts were introduced at $i = 201$ and are first detected at observations $i = 215$ and $i = 221$, respectively.

noise is so high that the model’s predictive power becomes very poor ($CV R^2 = 0.137$). However, as seen in Fig. 4.3b, our approach still successfully detects the concept drift, although there are post-shift periods over which the T^2 statistic temporarily drops below the CL.



(a) Low noise ($\sigma = 0.03$, 5-fold CV $R^2 \approx 0.975$) (b) High noise ($\sigma = 0.25$, 5-fold CV $R^2 \approx 0.137$)

Figure 4.4: Empirical pointwise false-alarm rate (PFAR) for the nonlinear oscillator example under low- and high-noise conditions. The dashed horizontal line indicates the nominal level $\alpha = 0.001$. Even under severe model misspecification (high noise), the bootstrap control limits maintain accurate pointwise false-alarm control prior to the change point.

Taken together, these results illustrate that the score-based monitoring approach remains effective even when the predictive model is a poor approximation to the true data-generating mechanism. Despite the neural network being only an approximation of the nonlinear dy-

namics in Eq. (4.4), changes in the underlying predictive relationship still induce a nonzero mean in the score vectors, leading to detectable shifts in the MEWMA statistic, as predicted by Eq. (2.4) and discussed in Zhang et al. (2023). Beyond detection behavior, Figure 4.4 further demonstrates that the proposed bootstrap control limits maintain accurate point-wise false-alarm control prior to the change point under both low- and high-noise conditions. In particular, even in the high-noise regime ($CV R^2 \approx 0.14$), the empirical PFAR remains close to $\alpha = 0.001$. This robustness is important in practice, since fitted machine learning models are invariably approximations of complex predictive relationships.

5 Conclusion

In this paper, we present a nested bootstrapping procedure to compute a time-varying CL for the score-based MEWMA control chart of Zhang et al. (2023), for detecting changes in the predictive distribution $\mathbb{P}(Y|\mathbf{X})$ represented by a supervised learning model. Our approach provides much more accurate false-alarm rate control than the approach of Zhang et al. (2023), especially with smaller training sample size n and/or larger desired FAR, and also produces a time-varying CL to maintain accurate false-alarm rate control prior to the MEWMA reaching steady state. Our derivations involve a non-obvious 0.632-type bootstrap correction that is essential for controlling the false-alarm rate.

Our approach provides much more accurate false-alarm rate control than the approach of Zhang et al. (2023), especially with smaller training sample size n and/or strict FAR (e.g., $\alpha = 0.001$). It is important to note that because our method uses the identical monitoring statistic as Zhang et al. (2023), the theoretical detection power for a given control limit is identical. The primary advantage of the proposed bootstrap method is the accurate calibration of that limit. Where the empirical quantile method of Zhang et al. (2023) tends to underestimate the limit in small samples (leading to excessive false alarms) or requires

massive holdout sets, our bootstrap correction ensures the nominal Type I error rate is maintained, allowing for valid monitoring even with limited data.

Disclosure statement

The authors have no conflicts of interest to declare.

References

- Abbasi, S. A., Yeganeh, A. & Shongwe, S. C. (2022), ‘Monitoring non-parametric profiles using adaptive EWMA control chart’, *Scientific Reports* **12**(14336).
- Apsemidis, A., Psarakis, S. & Moguerza, J. M. (2020), ‘A review of machine learning kernel methods in statistical process monitoring’, *Computers & Industrial Engineering* **149**, 106776.
- Baena-García, M., del Campo-Ávila, J., Fidalgo-Merino, R., Bifet, A., Gavaldà, R. & Morales-Bueno, R. (2006), Early drift detection method, *in* ‘Proceedings of the 4th ECML PKDD International Workshop on Knowledge Discovery from Data Streams (KDDSD)’, Springer, Berlin, Germany, pp. 77–86.
- Barocas, S., Hardt, M. & Narayanan, A. (2023), *Fairness and Machine Learning: Limitations and Opportunities*, MIT Press.
- Bickel, P. J. & Doksum, K. A. (2015), *Mathematical Statistics: Basic Ideas and Selected Topics*, Vol. 1 of *Chapman & Hall/CRC Texts in Statistical Science*, CRC Press, Boca Raton, FL.
- Chang, S. I. & Yadama, S. (2010), ‘Statistical process control for monitoring non-linear

- profiles using wavelet filtering and B-spline approximation’, *International Journal of Production Research* **48**(4), 1049–1068.
- Efron, B. (1983), ‘Estimating the error rate of a prediction rule: Improvement on cross-validation’, *Journal of the American Statistical Association* **78**(382), 316–331.
- Febbo, M. & Machado, S. P. (2013), ‘Nonlinear dynamic vibration absorbers with a saturation’, *Journal of Sound and Vibration* **332**(6), 1465–1483.
- Gama, J., Medas, P., Castillo, G. & Rodrigues, P. (2004), Learning with drift detection, in ‘Brazilian Symposium on Artificial Intelligence’, pp. 286–295.
- Gama, J., Žliobaitė, I., Bifet, A., Pechenizkiy, M. & Bouchachia, A. (2014), ‘A survey on concept drift adaptation’, *IEEE Transactions on Knowledge and Data Engineering* **27**(3), 701–720.
- Krawczyk, B., Minku, L. L., Gama, J., Stefanowski, J. & Wozniak, M. (2017), ‘Ensemble learning for data stream analysis: A survey’, *Information Fusion* **37**, 132–156.
- Malinovskaya, A., Mozharovskyi, P. & Otto, P. (2024), ‘Statistical process monitoring of artificial neural networks’, *Technometrics* **66**(1), 104–117.
- Montgomery, D. C. (2020), *Introduction to Statistical Quality Control*, 8th edn, John Wiley & Sons.
- Moreno-Torres, J. G., Raeder, T., Alaíz-Rodríguez, R., Chawla, N. & Herrera, F. (2012), ‘A unifying view on dataset shift in classification’, *Pattern Recognit.* **45**, 521–530.
- Psarakis, S. (2011), ‘The use of neural networks in statistical process control charts’, *Quality and Reliability Engineering International* **27**(5), 641–650.
- Razak, A. M. S., Nirmala, C. R., Sreenivasa, B. R., Lahza, H. & Lahza, H. F. M. (2023), ‘A

- survey on detecting healthcare concept drift in AI/ML models from a finance perspective’, *Frontiers in Artificial Intelligence* **5**, 955314.
- Ross, G. J., Adams, N. M., Tasoulis, D. K. & Hand, D. J. (2012), ‘Exponentially weighted moving average charts for detecting concept drift’, *Pattern Recognition Letters* **33**, 191–198.
- Steiner, S. H., Cook, R. J., Farewell, V. T. & Treasure, T. (2000), ‘Monitoring surgical performance using risk-adjusted cumulative sum charts’, *Biostatistics* **1**(4), 441–452.
- Sun, J., Fujita, H., Chen, P. & Li, H. (2017), ‘Dynamic financial distress prediction with concept drift based on time weighting combined with adaboost support vector machine ensemble’, *Knowledge-Based Systems* **120**, 4–14.
- Wang, H., Fan, W., Yu, P. S. & Han, J. (2003), Mining concept-drifting data streams using ensemble classifiers, *in* ‘KDD’, pp. 226–235.
- Webb, G. I., Hyde, R., Cao, H., Nguyen, H. L. & Petitjean, F. (2016), ‘Characterizing concept drift’, *Data Mining and Knowledge Discovery* **30**(4), 964–994.
- Woodall, W. H., Spitzner, D. J., Montgomery, D. C. & Gupta, S. (2004), ‘Using control charts to monitor process and product quality profiles’, *Journal of Quality Technology* **36**(3), 309–320.
- Yosinski, J., Clune, J., Bengio, Y. & Lipson, H. (2014), How transferable are features in deep neural networks?, *in* ‘Advances in Neural Information Processing Systems’, Vol. 27.
- Zhang, K., Apley, D. W. & Chen, W. (2021), ‘Nonstationarity analysis of materials microstructures via fisher score vectors’, *Acta Materialia* **211**, 116818.
- Zhang, K., Bui, A. T. & Apley, D. W. (2023), ‘Concept drift monitoring and diagnostics of supervised learning models via score vectors’, *Technometrics* **65**(2), 137–149.

Žliobaitė, I., Pechenizkiy, M. & Gama, J. (2016), ‘An overview of concept drift applications’,
Big data analysis: new algorithms for a new society pp. 91–114.

A Theoretical Derivations and Proofs

To derive the CLs presented in Section 3, we state the regularity and bootstrap assumptions used throughout. These conditions are standard for MLE-based score methods and bootstrap approximations.

A.1 Assumptions and Preliminary Results

Assumption A.1 (Model and MLE Regularity). *The training sample $\mathcal{D} = \{(\mathbf{x}_i, y_i)\}_{i=1}^n$ is drawn i.i.d. from a joint distribution $\mathbb{P}_0(Y, \mathbf{X})$ such that:*

- (i) **Correct specification:** *The supervised learning model $g_\gamma(\theta; \mathbf{x})$ induces a conditional density $\mathbb{P}(y | \mathbf{x}; \theta)$ that is correctly specified at a true parameter θ^0 .*
- (ii) **Identifiability:** *The parameter θ^0 is an identifiable element of the parametric family.*
- (iii) **Smoothness and Fisher information:** *The log-likelihood $\ell(\theta; \mathbf{x}, y) = \log \mathbb{P}(y | \mathbf{x}; \theta)$ is twice continuously differentiable in a neighborhood of θ^0 , and the Fisher information matrix $\mathbf{I}(\theta^0) = \mathbb{E}_0[-\nabla_\theta^2 \log \mathbb{P}(Y | \mathbf{X}; \theta^0)]$ exists, is finite, and satisfies $\mathbf{I}(\theta^0) \succ 0$.*
- (iv) **Score moments:** *The score vectors $\mathbf{s}(\theta^0; \mathbf{X}, Y) = \nabla_\theta \log \mathbb{P}(Y | \mathbf{X}; \theta)|_{\theta=\theta^0}$ have finite second moments.*
- (v) **Asymptotic normality of the estimator:** *The (possibly regularized) MLE $\hat{\theta}$ satisfies*

$$\sqrt{n}(\hat{\theta} - \theta^0) \xrightarrow{d} \mathcal{N}(\mathbf{0}, \mathbf{I}(\theta^0)^{-1}).$$

Assumption A.2 (The typical bootstrap assumption). *If \mathcal{D}^{new} is drawn from the same distribution as \mathcal{D} , the joint distribution of $(\mathcal{S}_{.368}^{new}, \bar{\mathbf{s}}, \widehat{\Sigma}, \widehat{\theta})$ is the same as the joint distribution of the analogous quantities $(\mathcal{S}_{OOB}^b, \bar{\mathbf{s}}^b, \widehat{\Sigma}^b, \widehat{\theta}^b)$ from the bootstrapping procedure,*

where \mathcal{S}_{368}^{new} is any randomly drawn subset of \mathcal{S}^{new} having the same cardinality $0.368n$ as \mathcal{S}_{OOB}^b .

Assumption A.3 (Misspecification regularity). Let \mathbb{P} denote a joint distribution of (\mathbf{X}, Y) , and let $p_\theta(y | \mathbf{x})$ be the working conditional density (possibly misspecified). Assume:

(i) **Existence and uniqueness of pseudo-true parameter:** The objective

$$M_{\mathbb{P}}(\theta) := \mathbb{E}_{\mathbb{P}}[\log p_\theta(Y | \mathbf{X})]$$

admits a unique maximizer $\theta_{\mathbb{P}}^*$ in the interior of a parameter space $\Theta \subset \mathbb{R}^p$.

(ii) **Differentiation under the expectation:** The function $\log p_\theta(y | \mathbf{x})$ is differentiable in θ , and

$$\nabla_{\theta} M_{\mathbb{P}}(\theta) = \mathbb{E}_{\mathbb{P}}[\mathbf{s}(\theta; \mathbf{X}, Y)],$$

with the interchange of gradient and expectation justified.

(iii) **Uniqueness of stationary point:** For $\mathbb{P} \in \{\mathbb{P}_0, \mathbb{P}_1\}$, the equation $\nabla_{\theta} M_{\mathbb{P}}(\theta) = \mathbf{0}$ has the unique solution $\theta = \theta_{\mathbb{P}}^*$.

Assumption A.4 (Monitoring process). New observations $(\mathbf{x}_{n+i}, y_{n+i})$ used for monitoring are drawn i.i.d. from the same in-control distribution $\mathbb{P}_0(Y, \mathbf{X})$ as the training data. Conditional on $\hat{\theta}$, the score vectors $\{\mathbf{s}_{n+i}\}_{i \geq 1}$ form an i.i.d. sequence with conditional mean $\mu(\hat{\theta})$ and conditional covariance $\mathbf{V}(\hat{\theta})$, as in equation (3.1).

Lemma A.1 (Moments of the MEWMA statistic under \mathbb{P}_0). Suppose Assumptions A.1 and A.4 hold, and that there is no concept drift so that the new observations $(\mathbf{x}_{n+i}, y_{n+i})$ are drawn i.i.d. from $\mathbb{P}_0(Y, \mathbf{X})$. Let $\{\mathbf{s}_{n+i}\}_{i \geq 1}$ and $\{\mathbf{z}_{n+i}\}_{i \geq 1}$ be the score vectors and MEWMA statistics defined in (3.1) and in Assumption A.4, respectively. Then,

for each $i \geq 1$,

$$\begin{aligned}\mathbb{E}_0[\mathbf{z}_{n+i} | \hat{\theta}] &= [1 - (1 - \lambda)^i] \mu(\hat{\theta}), \\ \text{Cov}_0[\mathbf{z}_{n+i} | \hat{\theta}] &= \frac{\lambda}{2 - \lambda} [1 - (1 - \lambda)^{2i}] \mathbf{V}(\hat{\theta}),\end{aligned}\tag{A.1}$$

where $\mu(\hat{\theta})$ and $\mathbf{V}(\hat{\theta})$ are the conditional mean and covariance of \mathbf{s}_{n+i} given $\hat{\theta}$ in (3.1).

Proof. By iterating the recursion $\mathbf{z}_{n+i} = \lambda \mathbf{s}_{n+i} + (1 - \lambda) \mathbf{z}_{n+i-1}$ with $\mathbf{z}_n = \mathbf{0}$, we obtain the moving-average representation

$$\mathbf{z}_{n+i} = \lambda \left[\mathbf{s}_{n+i} + (1 - \lambda) \mathbf{s}_{n+i-1} + (1 - \lambda)^2 \mathbf{s}_{n+i-2} + \cdots + (1 - \lambda)^{i-1} \mathbf{s}_{n+1} \right].$$

Conditional on $\hat{\theta}$, the score vectors $\{\mathbf{s}_{n+i}\}_{i \geq 1}$ are i.i.d. with mean $\mu(\hat{\theta})$ and covariance $\mathbf{V}(\hat{\theta})$ by (3.1). Taking conditional expectations and using linearity,

$$\mathbb{E}_0[\mathbf{z}_{n+i} | \hat{\theta}] = \lambda \sum_{k=0}^{i-1} (1 - \lambda)^k \mu(\hat{\theta}) = [1 - (1 - \lambda)^i] \mu(\hat{\theta}),$$

where we used the geometric-series identity $\sum_{k=0}^{i-1} (1 - \lambda)^k = [1 - (1 - \lambda)^i] / \lambda$.

For the covariance, conditional independence of the \mathbf{s}_{n+i} and the same moving-average representation give

$$\text{Cov}_0[\mathbf{z}_{n+i} | \hat{\theta}] = \lambda^2 \sum_{k=0}^{i-1} (1 - \lambda)^{2k} \mathbf{V}(\hat{\theta}) = \lambda^2 \frac{1 - (1 - \lambda)^{2i}}{1 - (1 - \lambda)^2} \mathbf{V}(\hat{\theta}).$$

Since $1 - (1 - \lambda)^2 = \lambda(2 - \lambda)$, this simplifies to

$$\text{Cov}_0[\mathbf{z}_{n+i} | \hat{\theta}] = \frac{\lambda}{2 - \lambda} [1 - (1 - \lambda)^{2i}] \mathbf{V}(\hat{\theta}),$$

which completes the proof. □

Combining Assumption A.2 with the conditional distribution in (3.1), the out-of-bag (OOB) score vectors associated with outer bootstrap replicate b satisfy

$$\mathbf{s}_{\text{OOB},i}^b \mid \hat{\theta}^b \stackrel{\text{i.i.d.}}{\sim} (\mu(\hat{\theta}^b), \mathbf{V}(\hat{\theta}^b)), \quad i = 1, 2, \dots, \quad (\text{A.2})$$

so that $\mathcal{S}_{\text{OOB}}^b$ plays the same role for $\hat{\theta}^b$ as an independent future sample \mathcal{S}^{new} would play for $\hat{\theta}$. Because a bootstrap resample contains on average $0.632n$ distinct points, its OOB set contains approximately $0.368n$ points. Thus, for each b we define the OOB mean and covariance as

$$\bar{\mathbf{s}}_{\text{OOB}}^b = \frac{1}{\lfloor 0.368n \rfloor} \sum_{i=1}^{\lfloor 0.368n \rfloor} \mathbf{s}_{\text{OOB},i}^b, \quad (\text{A.3})$$

$$\hat{\Sigma}_{\text{OOB}}^b = \frac{1}{\lfloor 0.368n \rfloor} \sum_{i=1}^{\lfloor 0.368n \rfloor} (\mathbf{s}_{\text{OOB},i}^b - \bar{\mathbf{s}}_{\text{OOB}}^b)(\mathbf{s}_{\text{OOB},i}^b - \bar{\mathbf{s}}_{\text{OOB}}^b)^\top. \quad (\text{A.4})$$

From (A.2), the sampling variability of the OOB mean is

$$\bar{\mathbf{s}}_{\text{OOB}}^b \mid \hat{\theta}^b \sim (\mu(\hat{\theta}^b), \mathbf{V}(\hat{\theta}^b) / \lfloor 0.368n \rfloor), \quad (\text{A.5})$$

and the expected OOB covariance satisfies

$$\mathbb{E}_0 \left[\hat{\Sigma}_{\text{OOB}}^b \mid \hat{\theta}^b \right] = \frac{\lfloor 0.368n \rfloor - 1}{\lfloor 0.368n \rfloor} \mathbf{V}(\hat{\theta}^b) \cong \mathbf{V}(\hat{\theta}^b), \quad (\text{A.6})$$

showing that $\bar{\mathbf{s}}_{\text{OOB}}^b$ and $\hat{\Sigma}_{\text{OOB}}^b$ behave like empirical mean and covariance based on a sample of size approximately $0.368n$ from the same population that generates future score vectors.

With these OOB quantities in hand, the inner bootstrap loop of Algorithm 1 treats $\mathcal{S}_{\text{OOB}}^b$ as the population from which future score vectors are generated. For each inner replicate j , a bootstrap sample $\{\mathbf{s}_i^{b,j}\}_{i \geq 1}$ is drawn with replacement from $\mathcal{S}_{\text{OOB}}^b$, and the corresponding

MEWMA statistic is defined recursively by

$$\mathbf{z}_i^{b,j} = \lambda \mathbf{s}_i^{b,j} + (1 - \lambda) \mathbf{z}_{i-1}^{b,j}, \quad \mathbf{z}_0^{b,j} = \mathbf{0}. \quad (\text{A.7})$$

This construction mirrors exactly the MEWMA definition for genuine future score vectors in Lemma A.1, except that the “future” population now has mean $\bar{\mathbf{s}}_{\text{OOB}}^b$ and covariance $\hat{\Sigma}_{\text{OOB}}^b$, each based on only $0.368n$ observations rather than n . Consequently, the MEWMA statistic $\mathbf{z}_i^{b,j}$ inherits an additional source of variability through the randomness of $\bar{\mathbf{s}}_{\text{OOB}}^b$. Lemma A.2 formalizes the resulting conditional mean and covariance of $\mathbf{z}_i^{b,j}$ and shows that, relative to the true MEWMA moments in Lemma A.1, an extra covariance term of order $[1 - (1 - \lambda)^i]^2 / (0.368n)$ appears.

Lemma A.2 (Conditional moments of bootstrap MEWMA statistic). *Suppose Assumption 3.2 holds, and let $\mathbf{z}_i^{b,j}$ denote the inner-bootstrap MEWMA statistic constructed from out-of-bag score vectors as in Algorithm 1. Then, for each outer replicate b and inner replicate j , the conditional mean and covariance of $\mathbf{z}_i^{b,j}$ given $\hat{\theta}^b$ satisfy*

$$\begin{aligned} \mathbb{E}_0[\mathbf{z}_i^{b,j} \mid \hat{\theta}^b] &= [1 - (1 - \lambda)^i] \mu(\hat{\theta}^b), \\ \text{Cov}_0[\mathbf{z}_i^{b,j} \mid \hat{\theta}^b] &\cong \left\{ \frac{\lambda}{2 - \lambda} [1 - (1 - \lambda)^{2i}] + \frac{1}{0.368n} [1 - (1 - \lambda)^i]^2 \right\} \mathbf{V}(\hat{\theta}^b), \end{aligned} \quad (\text{A.8})$$

for all $i \geq 1$.

Proof. Fix an outer bootstrap replicate b and its fitted parameter $\hat{\theta}^b$. By Assumption 3.2 and (A.2)–(A.6), the out-of-bag score vectors $\{\mathbf{s}_{\text{OOB},i}^b\}$ satisfy

$$\mathbf{s}_{\text{OOB},i}^b \mid \hat{\theta}^b \stackrel{\text{i.i.d.}}{\sim} (\mu(\hat{\theta}^b), \mathbf{V}(\hat{\theta}^b)),$$

and the OOB sample mean and covariance have conditional moments

$$\mathbb{E}_0[\bar{\mathbf{s}}_{\text{OOB}}^b \mid \hat{\theta}^b] = \mu(\hat{\theta}^b), \quad \mathbb{E}_0[\widehat{\Sigma}_{\text{OOB}}^b \mid \hat{\theta}^b] \cong \mathbf{V}(\hat{\theta}^b), \quad \text{Cov}_0[\bar{\mathbf{s}}_{\text{OOB}}^b \mid \hat{\theta}^b] \cong \frac{1}{0.368n} \mathbf{V}(\hat{\theta}^b).$$

For each inner bootstrap replicate j , the score vectors $\{\mathbf{s}_i^{b,j} : i = 1, 2, \dots\}$ are drawn with replacement from $\mathcal{S}_{\text{OOB}}^b$, so conditionally on $(\hat{\theta}^b, \mathcal{D}_{\text{OOB}}^b)$ they are i.i.d. with mean $\bar{\mathbf{s}}_{\text{OOB}}^b$ and covariance $\widehat{\Sigma}_{\text{OOB}}^b$. The corresponding inner-loop MEWMA statistic can be written as

$$\mathbf{z}_i^{b,j} = \lambda[\mathbf{s}_i^{b,j} + (1-\lambda)\mathbf{s}_{i-1}^{b,j} + (1-\lambda)^2\mathbf{s}_{i-2}^{b,j} + \dots + (1-\lambda)^{i-1}\mathbf{s}_1^{b,j}], \quad i = 1, 2, \dots$$

Applying the law of total expectation with respect to $\mathcal{D}_{\text{OOB}}^b$ gives

$$\begin{aligned} \mathbb{E}_0[\mathbf{z}_i^{b,j} \mid \hat{\theta}^b] &= \mathbb{E}_0\left[\mathbb{E}_0\left\{\lambda[\mathbf{s}_i^{b,j} + (1-\lambda)\mathbf{s}_{i-1}^{b,j} + \dots + (1-\lambda)^{i-1}\mathbf{s}_1^{b,j}] \mid \hat{\theta}^b, \mathcal{D}_{\text{OOB}}^b\right\} \mid \hat{\theta}^b\right] \\ &= \mathbb{E}_0\left[\lambda \sum_{k=0}^{i-1} (1-\lambda)^k \bar{\mathbf{s}}_{\text{OOB}}^b \mid \hat{\theta}^b\right] = \lambda \sum_{k=0}^{i-1} (1-\lambda)^k \mathbb{E}_0[\bar{\mathbf{s}}_{\text{OOB}}^b \mid \hat{\theta}^b] = [1 - (1-\lambda)^i] \mu(\hat{\theta}^b), \end{aligned} \tag{A.9}$$

which is exactly the first part of (A.8). Similarly, applying the law of total covariance with respect to $\mathcal{D}_{\text{OOB}}^b$ yields

$$\begin{aligned} \text{Cov}_0[\mathbf{z}_i^{b,j} \mid \hat{\theta}^b] &= \mathbb{E}_0\left[\text{Cov}_0\left(\lambda[\mathbf{s}_i^{b,j} + (1-\lambda)\mathbf{s}_{i-1}^{b,j} + \dots + (1-\lambda)^{i-1}\mathbf{s}_1^{b,j}] \mid \hat{\theta}^b, \mathcal{D}_{\text{OOB}}^b\right) \mid \hat{\theta}^b\right] \\ &\quad + \text{Cov}_0\left[\mathbb{E}_0\left(\lambda[\mathbf{s}_i^{b,j} + (1-\lambda)\mathbf{s}_{i-1}^{b,j} + \dots + (1-\lambda)^{i-1}\mathbf{s}_1^{b,j}] \mid \hat{\theta}^b, \mathcal{D}_{\text{OOB}}^b\right) \mid \hat{\theta}^b\right]. \end{aligned} \tag{A.10}$$

Conditionally on $(\hat{\theta}^b, \mathcal{D}_{\text{OOB}}^b)$, the score vectors $\mathbf{s}_i^{b,j}$ are i.i.d., so the first term becomes

$$\mathbb{E}_0\left[\lambda^2 \sum_{k=0}^{i-1} (1-\lambda)^{2k} \widehat{\Sigma}_{\text{OOB}}^b \mid \hat{\theta}^b\right] = \lambda^2 \sum_{k=0}^{i-1} (1-\lambda)^{2k} \mathbb{E}_0[\widehat{\Sigma}_{\text{OOB}}^b \mid \hat{\theta}^b] \cong \frac{\lambda}{2-\lambda} [1 - (1-\lambda)^{2i}] \mathbf{V}(\hat{\theta}^b).$$

The second term is the covariance of a linear combination of $\bar{\mathbf{s}}_{\text{OOB}}^b$, and using $\text{Cov}_0[\bar{\mathbf{s}}_{\text{OOB}}^b | \hat{\theta}^b] \cong \mathbf{V}(\hat{\theta}^b)/(0.368n)$ gives

$$\text{Cov}_0\left\{\lambda \sum_{k=0}^{i-1} (1-\lambda)^k \bar{\mathbf{s}}_{\text{OOB}}^b \mid \hat{\theta}^b\right\} \cong \frac{1}{0.368n} [1 - (1-\lambda)^i]^2 \mathbf{V}(\hat{\theta}^b).$$

Combining the two contributions yields

$$\text{Cov}_0[\mathbf{z}_i^{b,j} \mid \hat{\theta}^b] \cong \left\{ \frac{\lambda}{2-\lambda} [1 - (1-\lambda)^{2i}] + \frac{1}{0.368n} [1 - (1-\lambda)^i]^2 \right\} \mathbf{V}(\hat{\theta}^b),$$

which is exactly the second part of (A.8). This proves the stated expressions for the conditional mean and covariance of $\mathbf{z}_i^{b,j}$ given $\hat{\theta}^b$. \square

A.2 Proofs of Main Theorems

Proof of Theorem 3.1

Proof. From (A.9) and (A.10), applying the law of total expectation and the law of total covariance over $\hat{\theta}^b$ yields the unconditional mean and covariance of $\mathbf{z}_i^{b,j}$:

$$\mathbb{E}_0[\mathbf{z}_i^{b,j}] = \mathbb{E}_0\left[\mathbb{E}_0[\mathbf{z}_i^{b,j} \mid \hat{\theta}^b]\right] = [1 - (1-\lambda)^i] \mathbb{E}_0[\mu(\hat{\theta}^b)], \quad (\text{A.11})$$

and

$$\begin{aligned} \text{Cov}_0[\mathbf{z}_i^{b,j}] &= \mathbb{E}_0\left[\text{Cov}_0[\mathbf{z}_i^{b,j} \mid \hat{\theta}^b]\right] + \text{Cov}_0\left[\mathbb{E}_0[\mathbf{z}_i^{b,j} \mid \hat{\theta}^b]\right] \\ &= \left\{ \frac{\lambda}{2-\lambda} [1 - (1-\lambda)^{2i}] + \frac{1}{0.368n} [1 - (1-\lambda)^i]^2 \right\} \mathbb{E}_0[\mathbf{V}(\hat{\theta}^b)] \\ &\quad + [1 - (1-\lambda)^i]^2 \text{Cov}_0[\mu(\hat{\theta}^b)]. \end{aligned} \quad (\text{A.12})$$

To approximate the terms on the right-hand sides of (A.11) and (A.12) and relate them to (A.1), consider first-order Taylor expansions of $\mu(\hat{\theta}^b)$ and $\mathbf{V}(\hat{\theta}^b)$ about the true parameter

θ^0 . Assume $\mu(\theta)$ and $\mathbf{V}(\theta)$ are continuously differentiable in a neighborhood of θ^0 . Then

$$\mu(\hat{\theta}^b) \cong \mu(\theta^0) + \left[\nabla_{\theta}^{\top} \mu(\theta) \right]_{\theta=\theta^0} (\hat{\theta}^b - \theta^0). \quad (\text{A.13})$$

Using the standard likelihood identities at θ^0 , namely that the score has mean zero and $\mu(\theta^0) = \mathbf{0}$, and $[\nabla_{\theta}^{\top} \mu(\theta)]_{\theta=\theta^0} = -\mathbf{I}(\theta^0)$, equation (A.13) simplifies to

$$\mu(\hat{\theta}^b) \cong -\mathbf{I}(\theta^0)(\hat{\theta}^b - \theta^0).$$

Similarly,

$$\mathbf{V}(\hat{\theta}^b) \cong \mathbf{I}(\theta^0) + \left[\nabla_{\theta}^{\top} \mathbf{V}(\theta) \right]_{\theta=\theta^0} (\hat{\theta}^b - \theta^0), \quad (\text{A.14})$$

Under Assumption A.1, the MLE $\hat{\theta}$ satisfies the standard asymptotic normality, and the same holds for $\hat{\theta}^b$ by Assumption A.2. Combining this with (A.13)–(A.14) gives the approximations

$$\mathbb{E}_0 \left[\begin{pmatrix} \hat{\theta}^b \end{pmatrix} \right] \cong \mathbb{E}_0 \left[-\mathbf{I}(\theta^0) (\hat{\theta}^b - \theta^0) \right] \cong \mathbf{0}, \quad (\text{A.15})$$

$$\text{Cov}_0 \left[\begin{pmatrix} \hat{\theta}^b \end{pmatrix} \right] \cong \text{Cov}_0 \left[-\mathbf{I}(\theta^0) (\hat{\theta}^b - \theta^0) \right] \cong \mathbf{I}(\theta^0) \frac{\mathbf{I}^{-1}(\theta^0)}{n} \mathbf{I}(\theta^0) = \frac{\mathbf{I}(\theta^0)}{n}, \quad (\text{A.16})$$

and

$$\mathbb{E}_0 \left[\mathbf{V}(\hat{\theta}^b) \right] \cong \mathbb{E}_0 \left[\mathbf{I}(\theta^0) + \nabla_{\theta}^{\top} \mathbf{V}(\theta) \Big|_{\theta=\theta^0} (\hat{\theta}^b - \theta^0) \right] = \mathbf{I}(\theta^0). \quad (\text{A.17})$$

where the term involving $\nabla_{\theta}^{\top} \mathbf{V}(\theta)$ drops out in the expectation because $\mathbb{E}_0[\hat{\theta}^b - \theta^0] \approx \mathbf{0}$.

Substituting (A.15)–(A.17) into (A.11)–(A.12) yields

$$\mathbb{E}_0[\mathbf{z}_i^{b,j}] \cong \mathbf{0}, \quad \text{Cov}_0[\mathbf{z}_i^{b,j}] \cong \left\{ \frac{\lambda}{2-\lambda} [1 - (1-\lambda)^{2i}] + \frac{3.72}{n} [1 - (1-\lambda)^i]^2 \right\} \mathbf{I}(\theta^0). \quad (\text{A.18})$$

Using (A.1) and repeating the same Taylor and asymptotic arguments for $\hat{\theta}$ (rather than

$\hat{\theta}^b$) gives the analogous result for \mathbf{z}_i (now without the OOB mean-variability term),

$$\mathbb{E}_0[\mathbf{z}_i] \cong \mathbf{0}, \quad \text{Cov}_0[\mathbf{z}_i] \cong \left\{ \frac{\lambda}{2-\lambda} [1 - (1-\lambda)^{2i}] + \frac{1}{n} [1 - (1-\lambda)^i]^2 \right\} \mathbf{I}(\theta^0). \quad (\text{A.19})$$

Thus the unconditional covariance matrices of $\mathbf{z}_i^{b,j}$ and \mathbf{z}_i differ only by a scalar factor

$$\text{Cov}_0[\mathbf{z}_i^{b,j}] \cong k(\lambda, i, n) \text{Cov}_0[\mathbf{z}_i],$$

where $k(\lambda, i, n)$ is given by (3.3). This is exactly the relationship stated in Theorem 3.1. \square

Proof of Corollary 3.2

Proof. Theorem 3.1 implies that $\mathbb{E}_0(\mathbf{z}_i^{b,j}) \approx \mathbf{0}$ and $\text{Cov}_0(\mathbf{z}_i^{b,j}) \approx k(\lambda, i, n) \text{Cov}_0(\mathbf{z}_i)$. Thus the variance-corrected statistic $\tilde{\mathbf{z}}_i^{b,j} = \mathbf{z}_i^{b,j} / \sqrt{k(\lambda, i, n)}$ satisfies $\mathbb{E}_0(\tilde{\mathbf{z}}_i^{b,j}) \approx \mathbf{0}$ and $\text{Cov}_0(\tilde{\mathbf{z}}_i^{b,j}) \approx \text{Cov}_0(\mathbf{z}_i)$. Under the MLE asymptotics in Assumption A.1, both \mathbf{z}_i and $\tilde{\mathbf{z}}_i^{b,j}$ are asymptotically Gaussian with the same mean and covariance. Because Gaussian distributions are completely determined by their first two moments, the two vectors have the same limiting in-control distribution. The associated Hotelling statistics,

$$T_{n+i} = (\mathbf{z}_{n+i} - \bar{\mathbf{s}})^\top \hat{\Sigma}^{-1} (\mathbf{z}_{n+i} - \bar{\mathbf{s}}) \quad T_i^{b,j} = (\tilde{\mathbf{z}}_i^{b,j} - \bar{\mathbf{s}}^b)^\top (\hat{\Sigma}^b)^{-1} (\tilde{\mathbf{z}}_i^{b,j} - \bar{\mathbf{s}}^b),$$

therefore have asymptotically identical distributions under \mathbb{P}_0 . Assumption A.2 ensures that $(\bar{\mathbf{s}}^b, \hat{\Sigma}^b)$ mimic the distribution of $(\bar{\mathbf{s}}, \hat{\Sigma})$, so the collection $\{T_i^{b,j}\}$ provides a bootstrap sample from the same limiting law as T_{n+i} . Standard results for bootstrap quantile estimation then guarantee that the empirical $(1 - \alpha)$ upper quantile of $\{T_i^{b,j}\}$ consistently estimates the corresponding quantile of T_{n+i} . Thus setting CL_i equal to this empirical quantile gives $\mathbb{P}_0(T_{n+i} > \text{CL}_i) \approx \alpha$, yielding the desired pointwise false-alarm probabil-

ity. □

Proof of Theorem 3.3

Proof. Fix the Phase I training sample \mathcal{D} and condition on \mathcal{D} throughout. For each monitoring time $i \geq 1$, Algorithm 1 induces a two-stage bootstrap law $F_i(\cdot \mid \mathcal{D})$ for a generic bootstrap replicate T_i^* , and we write $q_{i,\alpha}(\mathcal{D})$ for its $(1 - \alpha)$ quantile.

Step 1: Geometric stabilization of the bootstrap MEWMA vector.

Consider a generic bootstrap replicate generated by Algorithm 1. Condition on the outer bootstrap resample (equivalently, condition on the fitted outer-bootstrap model and its OOB empirical distribution). In the inner loop, the resampled score stream $\{\mathbf{s}_t^*\}_{t \geq 1}$ is i.i.d. from the empirical OOB distribution, hence has finite second moment. In particular, under our standing assumptions there exists a finite constant $M_2(\mathcal{D}) < \infty$ such that

$$\mathbb{E}[\|\mathbf{s}_1^*\|^2 \mid \mathcal{D}] \leq M_2(\mathcal{D}). \quad (\text{A.20})$$

The bootstrap MEWMA recursion starts from $\mathbf{z}_0^* = 0$ and satisfies $\mathbf{z}_t^* = \lambda \mathbf{s}_t^* + (1 - \lambda)\mathbf{z}_{t-1}^*$ for $t \geq 1$. Unrolling the recursion yields the linear-filter representation

$$\mathbf{z}_i^* = \lambda \sum_{t=1}^i (1 - \lambda)^{i-t} \mathbf{s}_t^*, \quad i \geq 1. \quad (\text{A.21})$$

To formalize “steady state” for the same filter, let $\{\mathbf{s}_t^*\}_{t \in \mathbb{Z}}$ be a two-sided extension of the inner score stream such that, conditional on \mathcal{D} , it is i.i.d. with the same marginal law as \mathbf{s}_1^* . Define the stationary analogue of the same linear filter by

$$\mathbf{z}_{\infty,i}^* := \lambda \sum_{t=-\infty}^i (1 - \lambda)^{i-t} \mathbf{s}_t^*, \quad i \in \mathbb{Z}. \quad (\text{A.22})$$

(The series converges in L^2 because $\sum_{t=-\infty}^i (1-\lambda)^{2(i-t)} < \infty$ and $\mathbb{E}[\|\mathbf{s}_1^*\|^2 \mid \mathcal{D}] < \infty$.)

Subtracting (A.21) from (A.22) gives

$$\mathbf{z}_{\infty,i}^* - \mathbf{z}_i^* = \lambda \sum_{t=-\infty}^0 (1-\lambda)^{i-t} \mathbf{s}_t^* = \lambda(1-\lambda)^i \sum_{u=0}^{\infty} (1-\lambda)^u \mathbf{s}_{-u}^*,$$

where we substituted $u = -t$. Apply Minkowski's inequality in $L^2(\mathbb{P}(\cdot \mid \mathcal{D}))$:

$$\left(\mathbb{E} \left[\left\| \sum_{u=0}^{\infty} a_u \mathbf{s}_{-u}^* \right\|^2 \mid \mathcal{D} \right] \right)^{1/2} \leq \sum_{u=0}^{\infty} |a_u| (\mathbb{E}[\|\mathbf{s}_{-u}^*\|^2 \mid \mathcal{D}])^{1/2}.$$

Here $a_u := (1-\lambda)^u$. By conditional stationarity/i.i.d. of the two-sided extension, $\mathbb{E}[\|\mathbf{s}_{-u}^*\|^2 \mid \mathcal{D}] = \mathbb{E}[\|\mathbf{s}_1^*\|^2 \mid \mathcal{D}]$ for all u . Therefore,

$$\begin{aligned} (\mathbb{E}[\|\mathbf{z}_{\infty,i}^* - \mathbf{z}_i^*\|^2 \mid \mathcal{D}])^{1/2} &\leq \lambda(1-\lambda)^i \sum_{u=0}^{\infty} (1-\lambda)^u (\mathbb{E}[\|\mathbf{s}_1^*\|^2 \mid \mathcal{D}])^{1/2} \\ &= \lambda(1-\lambda)^i \cdot \frac{1}{\lambda} (\mathbb{E}[\|\mathbf{s}_1^*\|^2 \mid \mathcal{D}])^{1/2} \\ &= (1-\lambda)^i (\mathbb{E}[\|\mathbf{s}_1^*\|^2 \mid \mathcal{D}])^{1/2}. \end{aligned}$$

Combining this with (A.20), we obtain

$$(\mathbb{E}[\|\mathbf{z}_{\infty,i}^* - \mathbf{z}_i^*\|^2 \mid \mathcal{D}])^{1/2} \leq C_0(\mathcal{D}) (1-\lambda)^i, \quad C_0(\mathcal{D}) := (\mathbb{E}[\|\mathbf{s}_1^*\|^2 \mid \mathcal{D}])^{1/2}. \quad (\text{A.23})$$

Recall the variance-corrected statistic $\tilde{\mathbf{z}}_i^* = \mathbf{z}_i^* / \sqrt{k(\lambda, i, n)}$ from Corollary 3.2. Let $k_{\infty}(\lambda, n) := \lim_{i \rightarrow \infty} k(\lambda, i, n)$. Because $k(\lambda, i, n)$ is an explicit combination of terms $1 - (1-\lambda)^i$ and $1 - (1-\lambda)^{2i}$ (see (3.3)), there exists a constant $C_k < \infty$ (depending on λ, n) such that

$$|k(\lambda, i, n) - k_{\infty}(\lambda, n)| \leq C_k (1-\lambda)^i \quad \text{for all } i \geq 1. \quad (\text{A.24})$$

Moreover, $k(\lambda, i, n)$ is bounded away from zero and infinity uniformly in i , so there exists

$k_{\min} > 0$ such that $k(\lambda, i, n) \geq k_{\min}$ and $k_{\infty}(\lambda, n) \geq k_{\min}$. By the mean value theorem applied to $x \mapsto x^{-1/2}$ on $[k_{\min}, \infty)$,

$$\left| \frac{1}{\sqrt{k(\lambda, i, n)}} - \frac{1}{\sqrt{k_{\infty}(\lambda, n)}} \right| \leq \frac{1}{2} k_{\min}^{-3/2} |k(\lambda, i, n) - k_{\infty}(\lambda, n)| \leq C'_k (1 - \lambda)^i, \quad (\text{A.25})$$

for some finite $C'_k > 0$.

Define $\tilde{\mathbf{z}}_{\infty, i}^* := \mathbf{z}_{\infty, i}^* / \sqrt{k_{\infty}(\lambda, n)}$. Then, by adding and subtracting $\mathbf{z}_{\infty, i}^* / \sqrt{k(\lambda, i, n)}$ and using the triangle inequality,

$$\|\tilde{\mathbf{z}}_{\infty, i}^* - \tilde{\mathbf{z}}_i^*\| \leq \frac{1}{\sqrt{k(\lambda, i, n)}} \|\mathbf{z}_{\infty, i}^* - \mathbf{z}_i^*\| + \left| \frac{1}{\sqrt{k(\lambda, i, n)}} - \frac{1}{\sqrt{k_{\infty}(\lambda, n)}} \right| \|\mathbf{z}_{\infty, i}^*\|.$$

Taking conditional L^2 norms and using (A.23) and (A.25) together with $\sup_i \mathbb{E}[\|\mathbf{z}_{\infty, i}^*\|^2 \mid \mathcal{D}] < \infty$ (which follows from (A.20) and the square-summability of the filter weights), we conclude that there exists $C_1(\mathcal{D}) < \infty$ such that

$$(\mathbb{E}[\|\tilde{\mathbf{z}}_{\infty, i}^* - \tilde{\mathbf{z}}_i^*\|^2 \mid \mathcal{D}])^{1/2} \leq C_1(\mathcal{D}) (1 - \lambda)^i, \quad i \geq 1. \quad (\text{A.26})$$

Step 2: Geometric stabilization of the bootstrap T^2 statistic.

Define the (in-control) quadratic form

$$Q(\mathbf{z}) := (\mathbf{z} - \bar{\mathbf{s}})^\top \hat{\Sigma}^{-1} (\mathbf{z} - \bar{\mathbf{s}}),$$

where $\bar{\mathbf{s}}$ and $\hat{\Sigma}$ are the Phase I centering and covariance objects used in Corollary 3.2 (and hence are fixed when conditioning on \mathcal{D}). Let

$$T_i^* := Q(\tilde{\mathbf{z}}_i^*), \quad T_{\infty}^* := Q(\tilde{\mathbf{z}}_{\infty, i}^*).$$

Set

$$\mathbf{u} := \tilde{\mathbf{z}}_i^* - \bar{\mathbf{s}}, \quad \mathbf{v} := \tilde{\mathbf{z}}_{\infty,i}^* - \bar{\mathbf{s}}, \quad A := \hat{\Sigma}^{-1}.$$

Then $T_i^* = \mathbf{u}^\top A \mathbf{u}$ and $T_\infty^* = \mathbf{v}^\top A \mathbf{v}$.

For any matrix A and vectors \mathbf{u}, \mathbf{v} ,

$$|\mathbf{u}^\top A \mathbf{u} - \mathbf{v}^\top A \mathbf{v}| \leq \|A\| \|\mathbf{u} - \mathbf{v}\| (\|\mathbf{u}\| + \|\mathbf{v}\|), \quad (\text{A.27})$$

where $\|\cdot\|$ denotes the operator norm induced by the Euclidean norm. To verify (A.27), note that

$$\mathbf{u}^\top A \mathbf{u} - \mathbf{v}^\top A \mathbf{v} = (\mathbf{u} - \mathbf{v})^\top A \mathbf{u} + \mathbf{v}^\top A (\mathbf{u} - \mathbf{v}),$$

and apply Cauchy–Schwarz together with $\|A\mathbf{x}\| \leq \|A\| \|\mathbf{x}\|$ to each term.

Applying (A.27) with $A = \hat{\Sigma}^{-1}$ and using $\mathbf{u} - \mathbf{v} = \tilde{\mathbf{z}}_i^* - \tilde{\mathbf{z}}_{\infty,i}^*$ yields

$$|T_i^* - T_\infty^*| \leq \|\hat{\Sigma}^{-1}\| \|\tilde{\mathbf{z}}_i^* - \tilde{\mathbf{z}}_{\infty,i}^*\| \left(\|\tilde{\mathbf{z}}_i^* - \bar{\mathbf{s}}\| + \|\tilde{\mathbf{z}}_{\infty,i}^* - \bar{\mathbf{s}}\| \right). \quad (\text{A.28})$$

Take conditional expectation given \mathcal{D} in (A.28). Since $\hat{\Sigma}$ and $\bar{\mathbf{s}}$ are functions of \mathcal{D} , the quantity $\|\hat{\Sigma}^{-1}\|$ is deterministic under $\mathbb{P}(\cdot | \mathcal{D})$, hence

$$\mathbb{E}[|T_i^* - T_\infty^*| | \mathcal{D}] \leq \|\hat{\Sigma}^{-1}\| \mathbb{E}[X_i Y_i | \mathcal{D}],$$

where we define the nonnegative random variables

$$X_i := \|\tilde{\mathbf{z}}_i^* - \tilde{\mathbf{z}}_{\infty,i}^*\|, \quad Y_i := \|\tilde{\mathbf{z}}_i^* - \bar{\mathbf{s}}\| + \|\tilde{\mathbf{z}}_{\infty,i}^* - \bar{\mathbf{s}}\|.$$

By conditional Cauchy–Schwarz,

$$\mathbb{E}[X_i Y_i \mid \mathcal{D}] \leq (\mathbb{E}[X_i^2 \mid \mathcal{D}])^{1/2} (\mathbb{E}[Y_i^2 \mid \mathcal{D}])^{1/2}. \quad (\text{A.29})$$

Moreover, using $(a + b)^2 \leq 2a^2 + 2b^2$ gives

$$Y_i^2 \leq 2\|\tilde{\mathbf{z}}_i^* - \bar{\mathbf{s}}\|^2 + 2\|\tilde{\mathbf{z}}_{\infty,i}^* - \bar{\mathbf{s}}\|^2,$$

so $\mathbb{E}[Y_i^2 \mid \mathcal{D}] < \infty$ follows from the finite second moments of $\tilde{\mathbf{z}}_i^*$ and $\tilde{\mathbf{z}}_{\infty,i}^*$ established in Step 1. Consequently, we may define the (finite) constant

$$C_2(\mathcal{D}) := \|\hat{\Sigma}^{-1}\| \sup_{i \geq 1} (\mathbb{E}[Y_i^2 \mid \mathcal{D}])^{1/2} < \infty. \quad (\text{A.30})$$

Combining (A.28)–(A.30) yields

$$\mathbb{E}[|T_i^* - T_\infty^*| \mid \mathcal{D}] \leq C_2(\mathcal{D}) (\mathbb{E}[\|\tilde{\mathbf{z}}_i^* - \tilde{\mathbf{z}}_{\infty,i}^*\|^2 \mid \mathcal{D}])^{1/2}. \quad (\text{A.31})$$

Finally, apply the L^2 stabilization bound from Step 1, namely

$$(\mathbb{E}[\|\tilde{\mathbf{z}}_{\infty,i}^* - \tilde{\mathbf{z}}_i^*\|^2 \mid \mathcal{D}])^{1/2} \leq C_1(\mathcal{D})(1 - \lambda)^i,$$

to obtain

$$\mathbb{E}[|T_i^* - T_\infty^*| \mid \mathcal{D}] \leq C_3(\mathcal{D})(1 - \lambda)^i, \quad C_3(\mathcal{D}) := C_2(\mathcal{D})C_1(\mathcal{D}). \quad (\text{A.32})$$

Step 3: Quantile stabilization.

Let $F_i(\cdot \mid \mathcal{D})$ and $F_\infty(\cdot \mid \mathcal{D})$ denote the conditional CDFs of T_i^* and T_∞^* , and let $q_{i,\alpha}(\mathcal{D})$

and $q_{\infty,\alpha}(\mathcal{D})$ be their respective $(1 - \alpha)$ quantiles. Assume that the limiting bootstrap distribution $F_\infty(\cdot | \mathcal{D})$ admits a density $f_\infty(\cdot | \mathcal{D})$ and that there exist constants $\delta > 0$, $c_0(\mathcal{D}) > 0$, and $M(\mathcal{D}) < \infty$ such that

$$f_\infty(x | \mathcal{D}) \geq c_0(\mathcal{D}) \quad \text{for all } x \in [q_{\infty,\alpha}(\mathcal{D}) - \delta, q_{\infty,\alpha}(\mathcal{D}) + \delta],$$

and

$$\sup_x f_\infty(x | \mathcal{D}) \leq M(\mathcal{D}).$$

Under these conditions, a standard quantile perturbation argument yields

$$|q_{i,\alpha}(\mathcal{D}) - q_{\infty,\alpha}(\mathcal{D})| \leq \frac{1}{c_0(\mathcal{D})} \sup_x |F_i(x | \mathcal{D}) - F_\infty(x | \mathcal{D})|. \quad (\text{A.33})$$

To bound the CDF difference, fix $\eta > 0$. For any x ,

$$F_i(x | \mathcal{D}) \leq F_\infty(x + \eta | \mathcal{D}) + \mathbb{P}(|T_i^* - T_\infty^*| > \eta | \mathcal{D}),$$

and similarly,

$$F_\infty(x - \eta | \mathcal{D}) - \mathbb{P}(|T_i^* - T_\infty^*| > \eta | \mathcal{D}) \leq F_i(x | \mathcal{D}).$$

Combining the two bounds gives

$$\sup_x |F_i(x | \mathcal{D}) - F_\infty(x | \mathcal{D})| \leq \omega_\infty(\eta | \mathcal{D}) + \mathbb{P}(|T_i^* - T_\infty^*| > \eta | \mathcal{D}),$$

where

$$\omega_\infty(\eta | \mathcal{D}) := \sup_x \{F_\infty(x + \eta | \mathcal{D}) - F_\infty(x - \eta | \mathcal{D})\}.$$

By the uniform bound on the density $f_\infty(\cdot | \mathcal{D})$,

$$\omega_\infty(\eta | \mathcal{D}) = \sup_x \int_{x-\eta}^{x+\eta} f_\infty(u | \mathcal{D}) du \leq 2M(\mathcal{D})\eta.$$

Moreover, by Markov's inequality and the L^1 bound established in (A.32),

$$\mathbb{P}(|T_i^* - T_\infty^*| > \eta | \mathcal{D}) \leq \frac{\mathbb{E}[|T_i^* - T_\infty^*| | \mathcal{D}]}{\eta} \leq \frac{C_3(\mathcal{D})}{\eta}(1-\lambda)^i.$$

Choosing η proportional to $(1-\lambda)^i$ yields

$$\sup_x |F_i(x | \mathcal{D}) - F_\infty(x | \mathcal{D})| \leq C_4(\mathcal{D})(1-\lambda)^i,$$

for some finite constant $C_4(\mathcal{D})$ depending only on the Phase I training sample. Substituting this bound into (A.33) gives

$$|q_{i,\alpha}(\mathcal{D}) - q_{\infty,\alpha}(\mathcal{D})| \leq C(\mathcal{D})(1-\lambda)^i,$$

which establishes the desired geometric stabilization of the bootstrap control limit. This argument also implies existence and finiteness of $q_{\infty,\alpha}(\mathcal{D})$. \square

Proof of Theorem 3.4. Throughout, let

$$M_{\mathbb{P}}(\theta) := \mathbb{E}_{\mathbb{P}}[\log p_\theta(Y | \mathbf{X})], \quad \mathbf{s}(\theta; \mathbf{X}, Y) := \nabla_\theta \log p_\theta(Y | \mathbf{X}).$$

(a) By definition, θ^* maximizes $M_{\mathbb{P}_0}(\theta)$ over an open set and is an interior maximizer (Assumption A.3(i)), so the first-order optimality condition gives

$$\nabla_\theta M_{\mathbb{P}_0}(\theta^*) = \mathbf{0}.$$

By Assumption A.3(ii) (differentiation under the expectation),

$$\nabla_{\theta} M_{\mathbb{P}_0}(\theta) = \mathbb{E}_{\mathbb{P}_0}[\mathbf{s}(\theta; \mathbf{X}, Y)].$$

Evaluating at $\theta = \theta^*$ yields

$$\mathbb{E}_{\mathbb{P}_0}[\mathbf{s}(\theta^*; \mathbf{X}, Y)] = \mathbf{0}.$$

(b) Let θ_1^* denote the (unique) pseudo-true parameter under \mathbb{P}_1 , i.e., the unique maximizer of $M_{\mathbb{P}_1}(\theta)$ (Assumption A.3(i) under \mathbb{P}_1). Suppose, toward a contradiction, that

$$\mathbb{E}_{\mathbb{P}_1}[\mathbf{s}(\theta^*; \mathbf{X}, Y)] = \mathbf{0}.$$

By Assumption A.3(ii),

$$\nabla_{\theta} M_{\mathbb{P}_1}(\theta^*) = \mathbb{E}_{\mathbb{P}_1}[\mathbf{s}(\theta^*; \mathbf{X}, Y)] = \mathbf{0},$$

so θ^* is a stationary point of $M_{\mathbb{P}_1}$. By Assumption A.3(iii), the equation $\nabla_{\theta} M_{\mathbb{P}_1}(\theta) = \mathbf{0}$ has the unique solution $\theta = \theta_1^*$. Therefore $\theta^* = \theta_1^*$, which contradicts the assumption $\theta_1^* \neq \theta^*$.

Hence,

$$\mathbb{E}_{\mathbb{P}_1}[\mathbf{s}(\theta^*; \mathbf{X}, Y)] \neq \mathbf{0}.$$

(c) Define

$$\mu_1 := \mathbb{E}_{\mathbb{P}_1}[\mathbf{s}(\theta^*; \mathbf{X}, Y)],$$

which is nonzero by part (b). Consider the MEWMA recursion constructed from the score vectors $\mathbf{s}_i := \mathbf{s}(\theta^*; \mathbf{X}_i, Y_i)$ under \mathbb{P}_1 :

$$\mathbf{z}_i = \lambda \mathbf{s}_i + (1 - \lambda) \mathbf{z}_{i-1}, \quad \mathbf{z}_0 = \mathbf{0}.$$

Under \mathbb{P}_1 , $\{\mathbf{s}_i\}_{i \geq 1}$ are i.i.d. with mean μ_1 , so taking expectations in the recursion gives

$$\mathbb{E}_{\mathbb{P}_1}[\mathbf{z}_i] = \lambda\mu_1 + (1 - \lambda)\mathbb{E}_{\mathbb{P}_1}[\mathbf{z}_{i-1}], \quad \mathbb{E}_{\mathbb{P}_1}[\mathbf{z}_0] = \mathbf{0}.$$

Solving this linear difference equation yields

$$\mathbb{E}_{\mathbb{P}_1}[\mathbf{z}_i] = (1 - (1 - \lambda)^i)\mu_1 \xrightarrow{i \rightarrow \infty} \mu_1 \neq \mathbf{0},$$

and the convergence is geometric with rate $(1 - \lambda)$. This completes the proof. \square

B Computational Details and Additional Validation

This appendix provides additional computational details and validation results for the nonlinear oscillator example in Section 4.2, with a particular focus on pointwise false-alarm rate (PFAR) control and post-change detection behavior under varying noise levels.

B.1 Monte Carlo validation of PFAR

We conducted an independent Monte Carlo study to assess PFAR control for the nonlinear oscillator example. For each configuration, we generated $R = 8000$ independent monitoring streams from the in-control data-generating mechanism and recorded whether the monitoring statistic exceeded its corresponding time-varying control limit at each monitoring index i . The empirical PFAR at time i was computed as the fraction of runs that signaled at that time.

We considered two noise levels, $\sigma = 0.03$ (low noise) and $\sigma = 0.25$ (high noise), using identical monitoring parameters $\lambda = 0.01$ and nominal false-alarm rate $\alpha = 0.001$. Control limits were computed using the proposed nested bootstrap procedure with $B_O = 50$ outer bootstrap replicates and $B_I = 200$ inner bootstrap replicates. For each outer bootstrap replicate, the neural network was refit for 500 training epochs.

Figure 4.4 shows the resulting PFAR curves as functions of the monitoring index i for the low- and high-noise settings, respectively. During the in-control period ($i \leq 200$), the empirical PFAR remains close to the nominal level $\alpha = 0.001$ in both noise regimes, demonstrating accurate Type I error control even under severe model misspecification. After the change-point, the same curves reflect the pointwise probability of detection under concept drift and rise rapidly toward one, indicating strong eventual detectability.

B.2 Comparison with the two-sample control limits of Zhang et al. (2023)

For comparison, we conducted an analogous Monte Carlo study using the two-sample control-limit construction proposed by Zhang et al. (2023), implemented according to their recommended procedure. Figure B.1 summarizes the resulting PFAR and post-change detection behavior under low- and high-noise conditions, respectively.

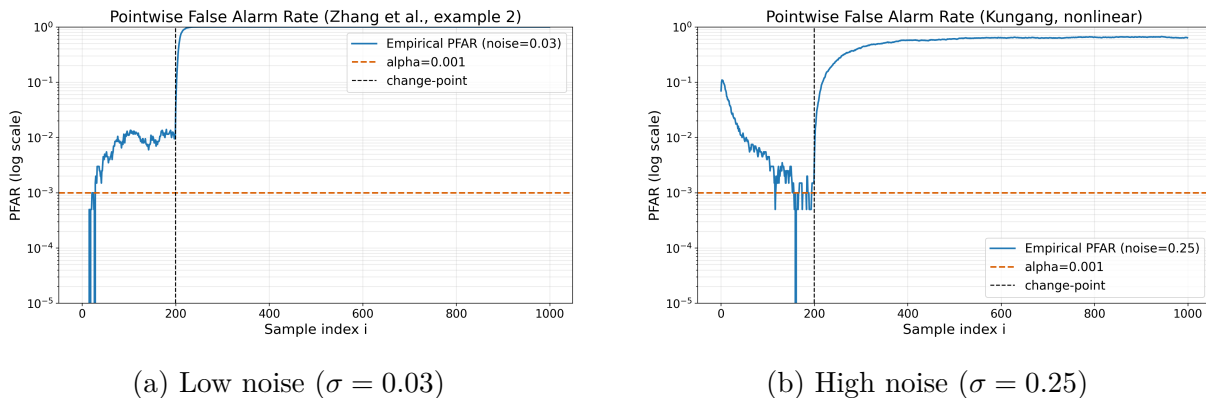


Figure B.1: Empirical pointwise false-alarm rate and post-change detection behavior for the two-sample control limits of Zhang et al. (2023) in the nonlinear oscillator example. Prior to the change-point ($i \leq 200$), the curves represent PFAR; after the change-point, they represent the pointwise probability of detection.

In the low-noise case ($\sigma = 0.03$), the two-sample method exhibits substantially inflated PFAR during the in-control period, often exceeding the nominal level by more than an order of magnitude. In the high-noise case ($\sigma = 0.25$), PFAR remains poorly controlled and highly variable, reflecting the difficulty of estimating extreme quantiles from a finite holdout sample in a low signal-to-noise regime.

In contrast, the proposed variance-corrected bootstrap control limits are calibrated to the full finite-sample variability of the monitoring statistic, accounting for both Phase I model-estimation uncertainty and Phase II monitoring variability. As a result, the bootstrap limits are appropriately positioned relative to the stationary post-change distribution of the MEWMA statistic, yielding eventual detection with probability approaching one even

in the high-noise regime.

B.3 Computational environment

All Monte Carlo experiments were executed on a shared high-performance computing cluster using a single compute node with 8 CPU cores and 32 GB of memory. Each PFAR experiment required approximately 6 hours and 46 minutes of wall-clock time. The hardware reported by the scheduler consisted of Intel Xeon Gold 6230R CPUs (2.10 GHz; 2 sockets, 26 cores per socket). No GPU resources were used. All computations were performed in Python 3.10.18 using a Conda environment, with PyTorch configured to run on CPU.